Empirical single-cell tracking and cell-fate simulation reveal dual roles of p53 in tumor suppression

Ann Rancourt[1,2], Sachiko Sato[1,3,4], and Masahiko S. Satoh[2,3,4]*

[1]Glycobiology and Bioimaging Laboratory of Research Center for Infectious Diseases and Research Centre of CHU de Québec, [2]Laboratory of DNA Damage Responses and Bioimaging, Research Centre of CHU de Québec, [3]The Bioimaging Platform of Research Centre of CHU de Québec and [4]Faculty of Medicine, Laval University, 2705 Boulevard Laurier, Québec, G1V 4G2, Canada

Corresponding author: Masahiko S. Satoh

TEL: 1-418-525-4444 ext. 47340

FAX: 1-418-654-2159

e-mail: masahiko.sato@crchudequebec.ulaval.ca

SUMMARY

The tumor suppressor p53 regulates various stress responses via increasing its cellular levels. The lowest p53 levels occur in unstressed cells; however, the impact of these low levels on cell integrity remains unclear. To address the impact, we used empirical single-cell tracking of p53-expressing and silenced cells, and developed a fate-simulation algorithm. Here we show that p53-silenced cells underwent more frequent cell death and cell fusion, which further induced multipolar cell division to generate aneuploid progeny. Those results suggest that the low levels of p53 in unstressed cells indeed have a role to maintain the integrity of a cell population. Results of a cell-fate simulation that provides a flexible and dynamic virtual culture space confirmed that these aneuploid progeny could propagate. However, p53-silenced cells were unable to propagate in a virtual cell population that was mainly comprised of p53-expressing cells, supporting the notion that p53 acts as a tumor suppressor. In contrast, when DNA damage responses were repeatedly induced in 53-expressed cells, p53-silenced cells became the major cell population, as the growth of p53-expressed cells was more tightly suppressed by the response than that of p53-silenced cells. In this context, p53-mediated damage response that is supposed to suppress tumor formation has a pro-malignant function. The cellular microenvironment could thus be a major factor to determine the fate of cancer cells and the fate-simulation algorithm can be used to reveal the fate.

INTRODUCTION

A healthy tissue architecture is maintained by homeostasis in normal cell populations [1]. However, the development of cancers within such an architecture implies that the cancer cells escape from this homeostasis by altering their functions and acquiring various cell abilities such as immortal growth and invasiveness [1]. The p53 gene is mutated in >50% of cancers [2-4], and loss of p53 function is considered to be involved in tumor progression, thereby defining *TP53* as a tumor suppressor gene [5, 6].

The cellular functions mediated by p53 are mainly related to its cellular level, which increases in response to stress, thus activating various mechanisms e.g. cell cycle arrest, cell senescence, cell death, and DNA damage responses [6-10]. Given that cell cycle arrest, cell senescence and cell death could lead to removal of the damaged cells, these processes could act to suppress tumor formation [7, 11-16]. The p53 levels are regulated via a mechanism mediated by Mdm2, which constantly degrades p53 by ubiquitination to maintain a low level until the cells are exposed to stress, when p53 accumulates as a result of its stabilization [5, 7, 8, 17-19]. These observations suggest that increased stress levels are required to elevate p53 levels sufficiently to allow it to exert its tumor suppressor function. Maintaining a background low level of p53 may thus have evolved as a means of allowing cells to respond quickly to stress. Alternatively, given that removing p53 by gene silencing increases the efficiency of induced pluripotent stem cell formation [20], maintaining a low level of p53 in unstressed cells *per se* may have functional implications. With this regard, it has been suggested that low levels of p53 activity may require normal cell growth to respond to a broad spectrum of stress [21] through suppression of apoptosis and regulation of metabolisms [5, 7, 22, 23]. However, the function of maintaining low levels of p53 in unstressed cells remains unclear.

Here, we investigated the effects of low levels of p53 on the behavior of cells using empirical single-cell tracking, to quantitatively evaluate the frequencies of cellular events, i.e. cell death (CD), aberrant cell divisions, and cell fusions (CF), which are difficult to be detected by lineage-reconstruction approaches that assume all cell divisions to be bipolar [24-26]. Spatiotemporal data obtained

by empirical tracking of individual cells treated with p53 siRNA and/or the alkylating agent *N*-methyl -*N′*-nitroso-*N*-nitrosoguanidine (MNNG) were also used. Furthermore, to follow the fate of individual cells in a cell population, we developed a cell-fate simulation algorithm based on empirical single-cell tracking data. Our results suggest that the low levels of p53 in unstressed cells indeed have a role to maintain the integrity of a cell population, thereby leading p53-silenced cells to aberrant cellular events. A cell-fate simulation analysis revealed that those p53-silenced cells were unable to propagate. In contrast, in the condition where DNA damage was repeatedly introduced to a cell population composed of 4% p53-silenced cells and 96% of p53-proficient cells, p53-silenced cells became the major cell population. In this context, damage response that is supposed to suppress tumor formation is instead involved in a pro-malignant process. The fate of cancer cells could thus be influenced by their complex microenvironment and our system could be used to reveal the unexpected fate of cancer cells in the environment.

RESULTS

System to investigate the functional implications of maintaining a low level of p53 in unstressed cells

We developed a system to determine if the low level of p53 retained in unstressed cells had a functional role in maintaining the integrity of a cell population. The level of p53 may only have a subtle effect on cell behavior, and we therefore analyzed the behaviors of individual cells by concurrent video recording of A549 p53 proficient lung carcinoma cells treated with scrambled small interfering RNA (siRNA) or p53 siRNA (Fig. 1). Responses of cells to MNNG were also monitored by concurrent video recording. To start tracking individual cells, progenitors were selected in video images at a tracking time of 0 min, and empirical single-cell tracking of progenitors and their progeny was performed by identifying cellular events including bipolar cell division (BD), tripolar cell division, tetrapolar cell division (tripolar and tetrapolar divisions were defined as multipolar division, MD), CD, and CF (see Fig. S1 for still images of BD, MD, CD and CF; corresponding videos were deposited in Dryad). A set of cell-lineage data (cell-lineage dataset) was thus composed of spatiotemporal cell tracking data and events that occurred in the tracked cells. Cell-lineage maps were generated from the set. The cell-lineage database contained multiple cell-lineage datasets, thereby allowing quantitative bioinformatics analyses. The database was also used for the development of a fate-simulation algorithm.

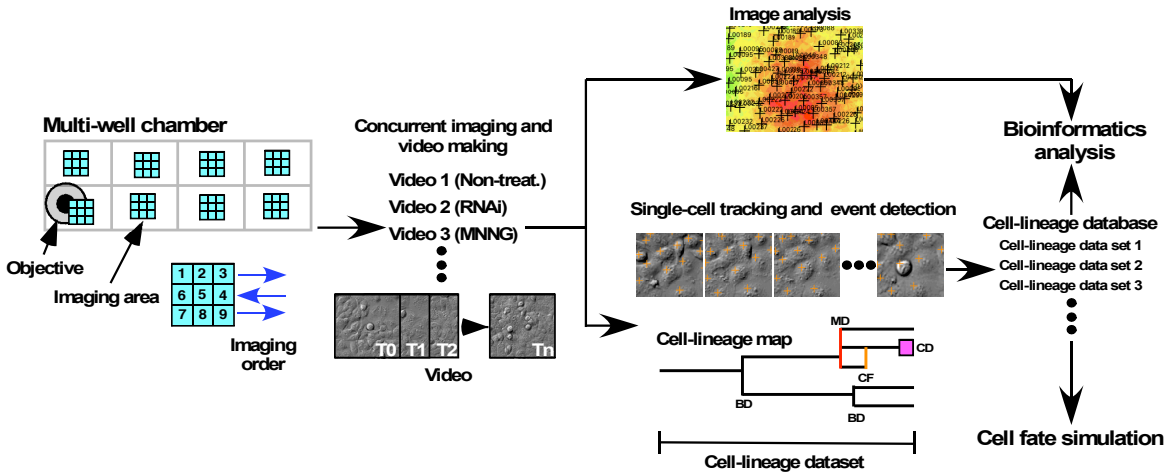

Figure 1. System for investigating the functional implications of maintaining low cell levels of p53. A549 cells were cultured on multi-well chamber slides and the areas of interest were scanned. Cells were treated with scrambled siRNA or p53 siRNA in the presence or absence of various doses of MNNG, and the cell responses were monitored to generate live cell imaging videos. The videos were used for imaging and single-cell tracking, starting immediately after MNNG treatment. Progenitors were selected from the image designated as tracking time 0 min (T0), and the progenitors and their progeny were tracked empirically. Each cell-linage dataset comprised tracking results for one progenitor and their progeny, and any events that occurred in the cells. A cell-lineage map was generated from the dataset, and the cell-lineage database contains multiple cell-lineage datasets. Quantitative bioinformatics analysis was performed using the database, which was also used to develop a cell-fate simulation algorithm.

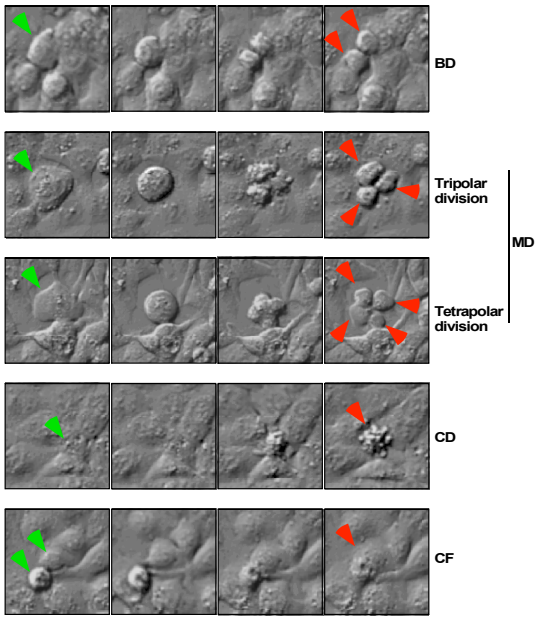

Supplementary Figure 1. Events occurring in the cells. Cellular events that occurred in A459 cells were categorized as follows: bipolar cell division (BD), tripolar cell division, tetrapolar cell division, cell death (CD), and cell fusion (CF). In the current study, tripolar and tetrapolar cell divisions were defined as multipolar cell division (MD). Green arrowheads indicate cells that underwent an event. Red arrowheads indicate daughter cells, a dead cell, and a fused cell.

Density of A549 cells

There is currently no standard protocol for single-cell tracking analysis using RNA interference (RNAi). We therefore examined some critical experimental parameters. First, we prepared uniform cell cultures for siRNA treatment using plated cells occupying ~90% of the culture surface within 24 h. However, because this condition may cause over-confluency of cells, we confirmed that these cells could continue to grow during video monitoring at this density by creating cell density maps at each imaging time point (Fig. S2a for still images and Movie S1) by assigning a value of 1 to pixels within a 20-pixel diameter of the position of the cell (Fig. S2b). If an area overlapped with other areas, the pixel was assigned the sum of the number of overlapped areas. These values were converted into a heat map, which showed an increase in density during video monitoring (Fig. S2a and Movie S1). Cell density increased linearly and average cell size was reduced (Fig. S2c), suggesting that the culture conditions used does not reduce cell growth during monitoring.

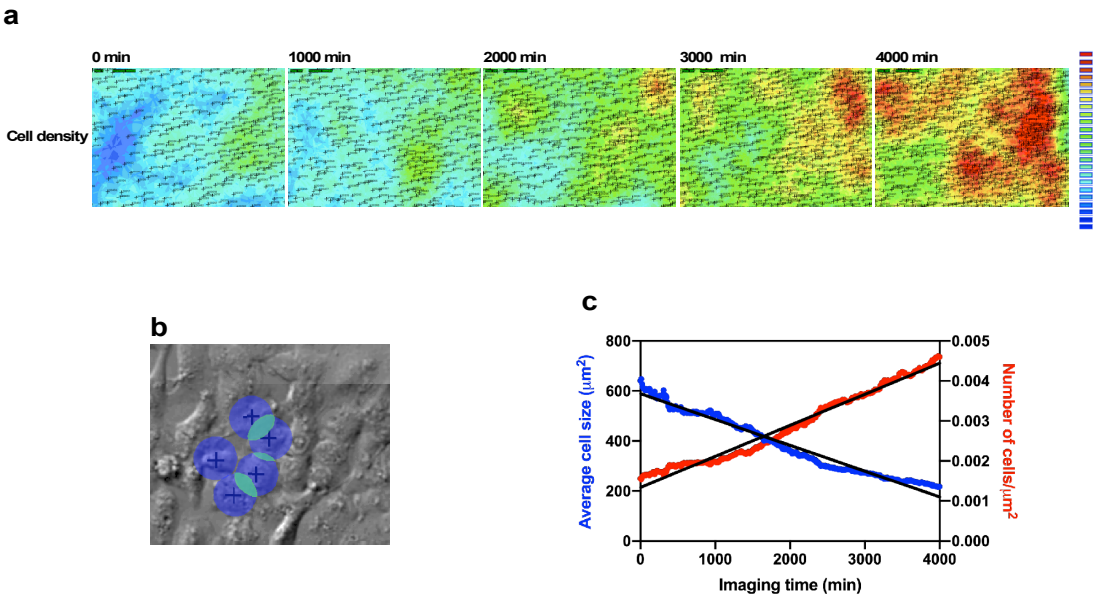

Supplementary Figure 2. Cell-density analysis. Cell density maps were created using a heat map scale. (**a**) Still images taken from Movie S1. Cell density map created by assigning value 1 to a pixel within the 20-pixel diameter area from the position of a cell (blue); if an area overlapped with other areas, the pixel was assigned the sum of the number of overlapped areas (light green) (**b**). These values were used to generate heat maps. Cell density and average cell size every 10 min were plotted (**c**).

Minimum number of cell-lineage datasets required to build a cell-lineage database

We also determined the minimum number of cell-lineage datasets needed to build a cell-lineage database with reproducible results. We constructed cell-lineage databases with 50–240 cell-lineage datasets. For example, 50 cell-lineage datasets were randomly selected to build a cell-lineage database, and this selection was repeated three times for triplicate analysis. Cell population expansion curves were then generated to assess analytical variation. The results for 50, 80, 120, 140, and 240 cell-lineage datasets are shown in Fig. S3a-e. Plotting growth variation at a tracking time of 4,000 min showed that the variations tended towards a plateau when >240 cell-lineage datasets were used (Fig. S3f). This suggests that >240 cell-lineage datasets are sufficient for reproducible single-cell tracking analysis, and we therefore used a cell-lineage database with 335 cell-lineage datasets.

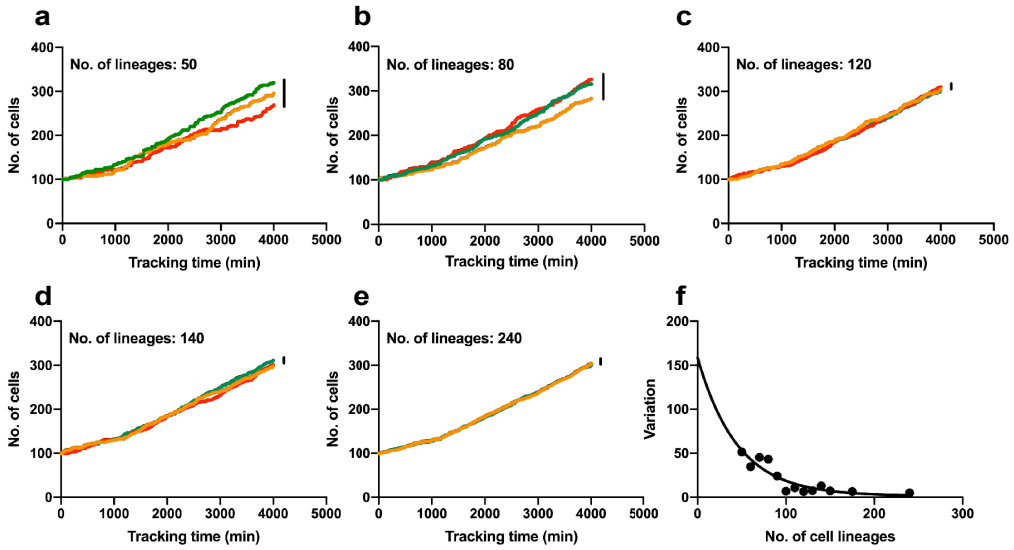

Supplementary Figure 3. Determination of minimum number of cell-lineage datasets required to build a cell-lineage database. A cell-lineage database containing 50–240 cell-lineage datasets was used to determine cell population expansion curves. (**a-e**) Cell population expansion curves determined based on cell-lineage databases containing 50 (**a**), 80 (**b**), 120 (**c**), 140 (**d**), and 240 (**e**) datasets. The number of cells every 10 min was calculated using the database and plotted. The analysis was repeated three times (green, orange, and red lines) to show variations at a tracking time of 4,000 min (black bars). (**f**) Variations of 4,000 min were plotted.

Silencing of p53 and single-cell tracking

We determined the length of time required for single-cell tracking following siRNA transfection. Because transfection can be monitored by observing the accumulation of particles (transfection reagents) in cells (Fig. S4a, differential interference contrast image, DIC), we quantitated the number of particles in an area of the cell culture by extracting particles brighter than 150 out of a 254 grayscale from the video image, and counted the number of particles with a size of 5–30 pixels (Fig. S4a, Particles, and Movie S2). The number of particles started to increase at about 1,200 min (20 h) after transfection and peaked at 3,750 min (62.5 h) (Fig. S4b). Western blotting analysis performed 48 h after transfection confirmed silencing of p53 (Fig. S4c; Control *vs.* p53, ~70% reduction) and the occurrence of p53 stabilization by exposure of cells to 7 μM MNNG (5.8-fold increase). Based on these parameters, we applied a 30-min pulse of MNNG treatment after the start of particle accumulation (Fig. S4b; 1,740 min (29 h) after transfection). Single-cell tracking was started at the end of MNNG treatment and continued for 4,000 min (66.7 h), by which time the number of particles was reduced to 70% of that at the peak.

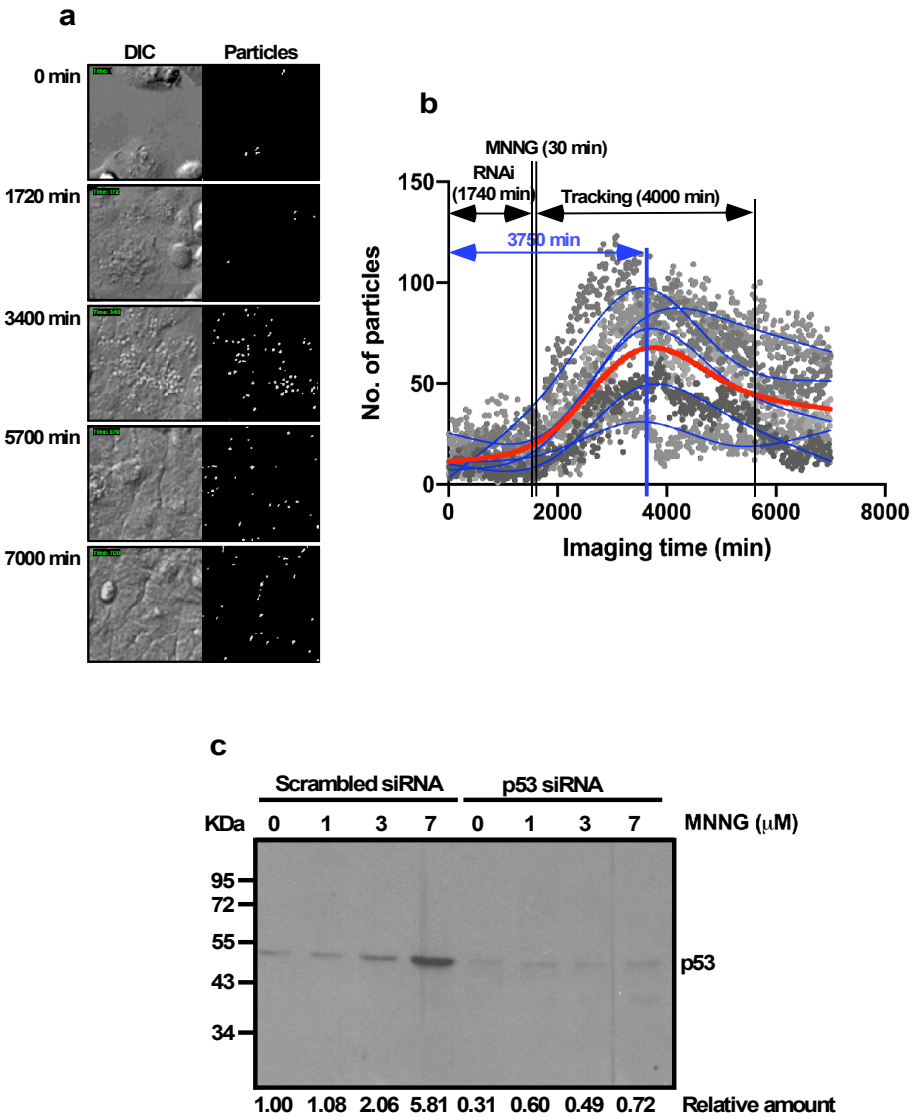

Supplementary Figure 4. Accumulation of particles following siRNA transfection and analysis of p53 expression following transfection and/or MNNG exposure. (**a**) Particles formed following siRNA transfection are shown. DIC and objects with brightness 150–254 and size 5–30 pixels were extracted from the DIC image (Particles). (**b**) The numbers of particles at five different locations in the image were plotted. Blue lines represent the average number of particles at each time point and the red line shows the overall average. MNNG treatment was performed after approximately 1,740 min of siRNA transfection, and continued for 30 min. The number of particles peaked at 3,750 min after transfection. Single-cell tracking was started immediately after MNNG treatment and continued for 4,000 min. (**c**) Western blotting with anti-p53 antibody was performed 48 h after siRNA treatment. Amounts of p53 relative to Control are shown.

Effect of silencing the low levels of p53 on cell population expansion

The lowest levels of p53 could occur in unstressed cells [5, 7, 8, 17-19]. To gain insights into the functions of such low levels of p53, we analyzed the expansion rate of a p53-silenced cell population and their response to MNNG exposure using empirical single-cell tracking analysis. To obtain reference data to

verify the results of the tracking analysis, we also measured the expansion rate by counting the number of cells using videos. To this end, images were divided into 5 × 5 squares (~512 × 512 pixels per square) and the number of cells within a square was determined at 1,000-min intervals (Fig S5). We used three independently generated videos with multiple squares from each. The results of counting the cells transfected with scrambled siRNA (Control) and p53 siRNA (p53si) are summarized in Fig. 2a and b, respectively. The rates of expansion of the Control and p53si cells and their responses to MNNG exposure were also compared (Fig. 2c-f). There was no significant difference in expansion rate between Control and p53si cells (Fig. 2c). There were no significant changes in expansion rate in Control cells exposed to 1 μM MNNG (Fig. 2a, Control vs. MNNG1). In contrast, the expansion rate of p53si-MNNG1 cells was significantly lower than that of MNNG1 cells (Fig. 2d). The expansion rates of both Control and p53si cells was reduced by exposure to 3 μM MNNG (Fig. 2e, MNNG3 and p53si-MNNG3), and similar to p53si-MNNG1 cells, the rate of p53si-MNNG3 cells was significantly lower than that of MNNG3 cells. Finally, 7 μM MNNG, which stabilized p53 (Fig. S4c), significantly reduced the expansion rates of the Control and p53si cells (Fig. 2f). In contrast to 1 and 3 μM MNNG exposure, MNNG7 cells showed slower expansion than p53si-MNNG cells.

Single-cell tracking analysis yielded similar results to the classical counting method (Fig. 2g-l; videos of the single-cell tracking processes, cell lineage maps and cell lineage data sets were deposited in Dryad). Overall, these results suggest that some alteration occurs in p53si cells. Given that the rate of cell population expansion can be affected by various factors, we further analyzed individual cells and cell lineages recorded in the cell-lineage database.

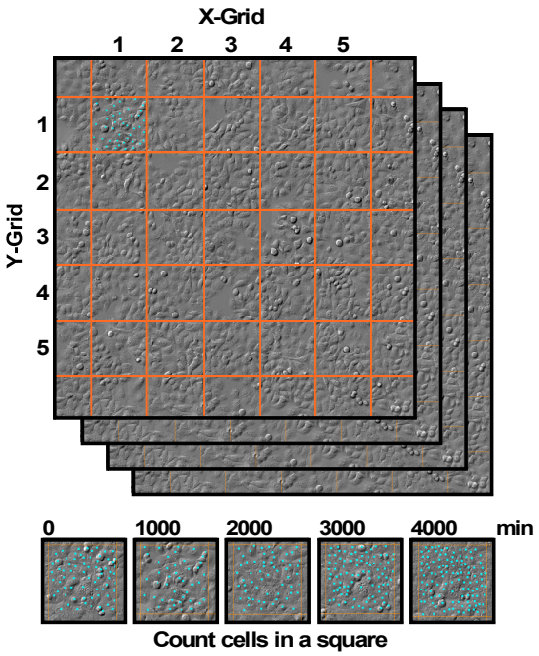

Supplementary Figure 5. Determination of cell-population expansion rate using video images. A video image (typically 2560 pixels x 2560 pixels) was divided into 5 x 5 squares and the numbers of cells in selected squares were counted. Counting was performed every 1,000 min in video images from 0-4,000 min.

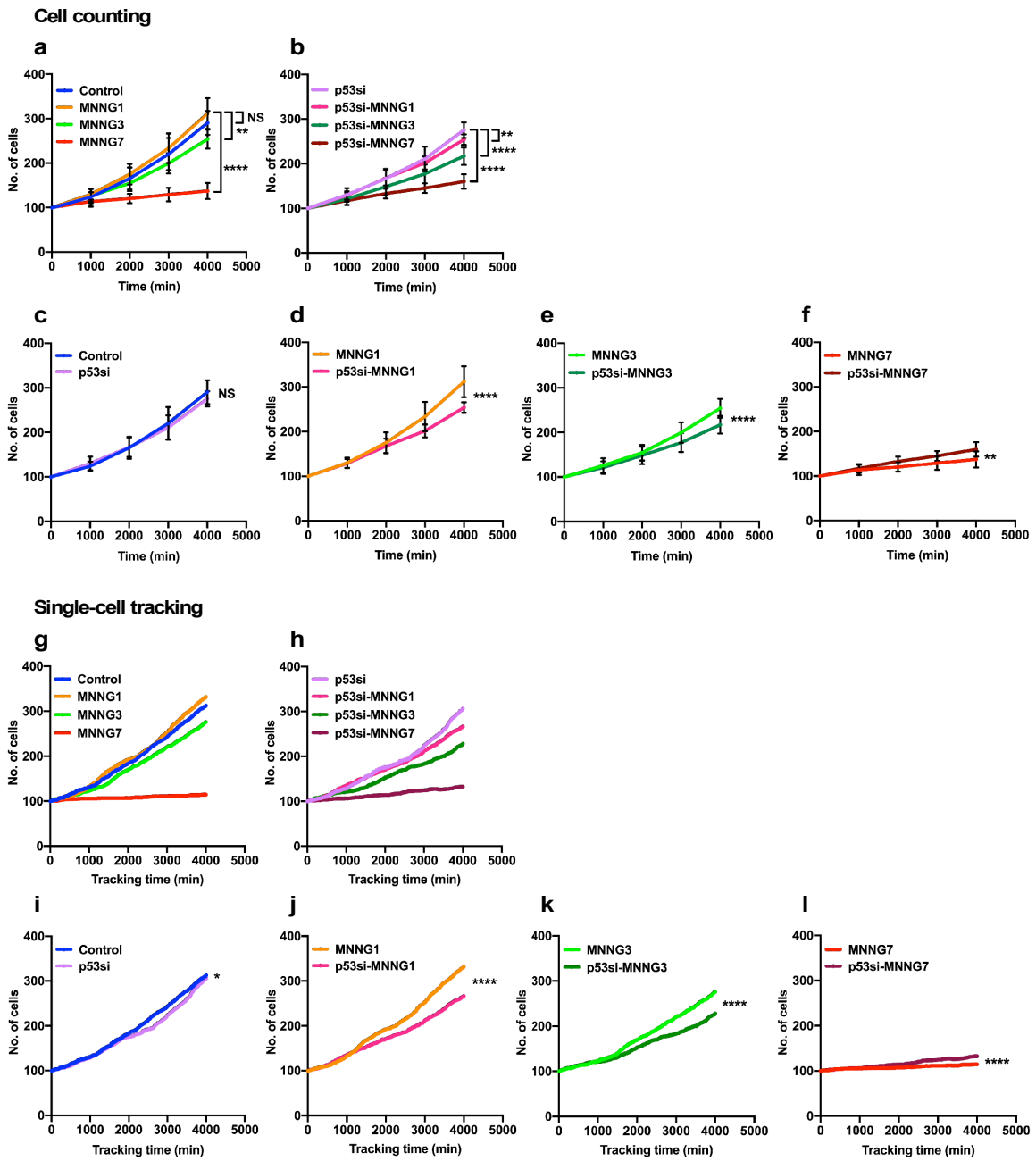

Figure 2. Cell-population expansion rates determined by cell counting and single-cell tracking analysis. Control (**a**) and p53si (**b**) cells were exposed to 1, 3, and 7 µM MNNG to give Control and MNNG1, MNNG3, and MNNG7 cells, and p53si and p53si-MNNG1, p53si-MNNG3, and p53si-MNNG7 cells, respectively. (**a-f**) Images were divided into a 5 x 5 squares and cell population expansion curves were determined by counting the number of cells in a square (~ 512 x 512) at 1,000 min intervals (see Fig. S5). Fifteen squares were selected from three independently generated videos. Expansion curves were compared as follows: Control vs. p53si (**c**), MNNG1 vs. p53si-MNNG1 (**d**), MNNG3 vs. p53si-MNNG3 (**e**), and MNNG7 vs. p53si-MNNG7 (**f**) cells. Student's t-test (**c-f**) and ordinary one-way ANOVA (Tukey's) (**a** and **b**) were performed (n=15), and standard errors are shown. (**g** and **h**) Cell population expansion curves of Control (**g**) and p53si (**h**) cells were determined using a cell-lineage database. Single-cell tracking was performed for 4,000 min with videos acquired at 10 min intervals (n=399). The number of cells every 10 min was calculated and plotted. Growth curves were compared as follows: Control vs. p53si (**i**), MNNG1 vs. p53si-MNNG1 (**j**), MNNG3 vs. p53si-MNNG3 (**k**), and MNNG7 vs. p53si-MNNG7 (**l**) cells. (**i-l**) The data were analyzed by Student's t-tests in the following approach. The difference in cell numbers between n and n+10 min was calculated (e.g. if the numbers of cells at 10 and 20 min were 100 and 103, the difference was 3). (**a-f** and **i-l**) NS: non-significant, *P < 0.05, **P < 0.01, ***P < 0.001, ****P < 0.0001.

Number of progeny produced from a progenitor

To gain further insights into p53si cells and cells exposed to MNNG, we analyzed the number of progeny produced from a progenitor cell using a cell-lineage database (Fig. 3a and b). Examples of the data analysis are shown in Fig. 3c. If a progenitor produced two progeny at the end of cell tracking, the lineage was categorized according to the number of progeny/lineage as 1–3, and 2 was added to the lineage category; similarly, if four progeny were produced, the cell lineage was categorized as 4–6, and 4 was added to this lineage category. This allowed us to determine which progenitors, i.e. highly or poorly reproductive ones, contributed to the maintenance of the cell population. In Control cells, the main cells contributing to maintaining the cell population were progenitors that produced 7–9 progeny (Fig. 3a). Differences in cell numbers relative to Control cells could thus further highlight the characteristics of each treatment (Fig. 3b). For example, suppression of population expansion in cells exposed to 3 or 7 μM MNNG could be explained by a reduction in progenitors that produced e.g. 7–9 progeny. In contrast, p53si cells were expected to generate a larger population compared with Control cells because of an increase in progenitors able to generate 10–12 progeny (Fig. 3b). However, the results showed similar or smaller sized cell populations of p53si and Control cells at a tracking time of 4,000 min (Fig. 2c and i), suggesting the occurrence of a cellular event that counteracts the expansion of the cell population in p53si cells.

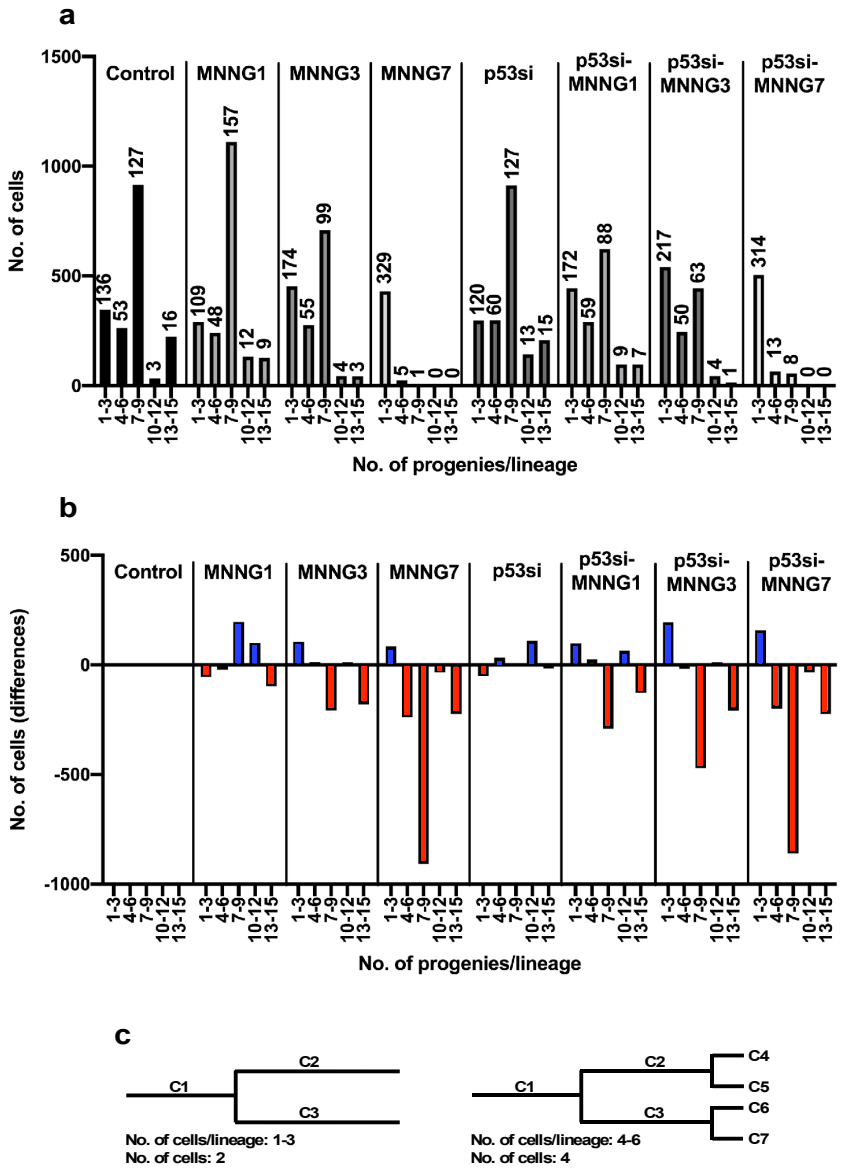

Figure 3. Number of progeny produced from a progenitor. (**a**) The number of progeny produced from a progenitor was calculated, as shown in (**c**). If a progenitor produced two progeny at a tracking time of 4,000 min, this lineage was categorized as No. of progenies/lineage = 1–3, with No. of cells = 2. Similarly, if four progeny were produced, the lineage was categorized as No. of progenies/lineage = 4–6, and No. of cells = 4. Values shown in (**a**) are number of lineages. (**c**) Differences relative to the No. of Control cells were also calculated. Blue and red bars represent groups in the cell lineage that were increased (blue) or decreased (red) relative to the Control cells after silencing and/or MNNG treatment.

Impact of p53-silencing on aberrant cellular events

We focused on MD, CD, and CF events, to gain an insight into the impact of events occurring in p53si cells on expansion of the cell population. To this end, we first visually inspected each time point of the video image and counted the number of events, in addition to analysis using a cell-lineage database. CF

tends to occur gradually and was therefore difficult to detect without single-cell tracking analysis, and only MD and CD events were counted by visual inspection. Each time point of the video image was divided into four squares (Fig. S6a) and the numbers of CD and MD events in each square were marked in three independently generated videos. We also prepared images by stacking the positions of MD and CD events to create MD and CD density maps, using a similar approach to that used for cell density determination (Fig. S2b). MD density maps (Fig. S6b) showed that p53 silencing significantly increased MD density relative to Control cells (Fig. S6b), and MD density was reduced by MNNG treatment. Similarly, CD density was increased by p53 silencing (Fig. S6c; Control vs. p53si cells) but was also increased by exposure to 7 μM MNNG. We analyzed the results statistically, and confirmed that p53 silencing significantly increased MD events, and this was counteracted by MNNG (Fig. 4a). The p53 silencing also significantly induced CD (Fig. 4b), and this was further promoted by exposure to 7 μM MNNG. Single-cell tracking analysis (Fig. 4c and d) yielded consistent results with counting. With regard to the induction of CD by 7 μM MNNG, the difference in number of CD events between the Control and MNNG7 cells determined by counting was higher than that determined by single-cell tracking analysis. This was because the area of single-cell tracking was slightly outside the area where CDs frequently occurred (Fig. S6c). Detection of CF required the fused cells to be followed-up for at least 30 time points (~5 h) to confirm the occurrence of CF, and single-cell tracking analysis also revealed that silencing p53 increased the frequency of CF, and this was counteracted by MNNG (Fig. 4e). Taken together, these results suggested that the low levels of p53 retained in unstressed cells function to suppress MD, CD, and CF, and these events were thus induced following p53 silencing. Although silencing induced those events, the chances of detecting MD, CD, and CF were as low as 0.0475, 0.125, and 0.0775 events per 10 min/300 lineages, respectively, implying that accurate detection of those events requires empirical single-cell tracking.

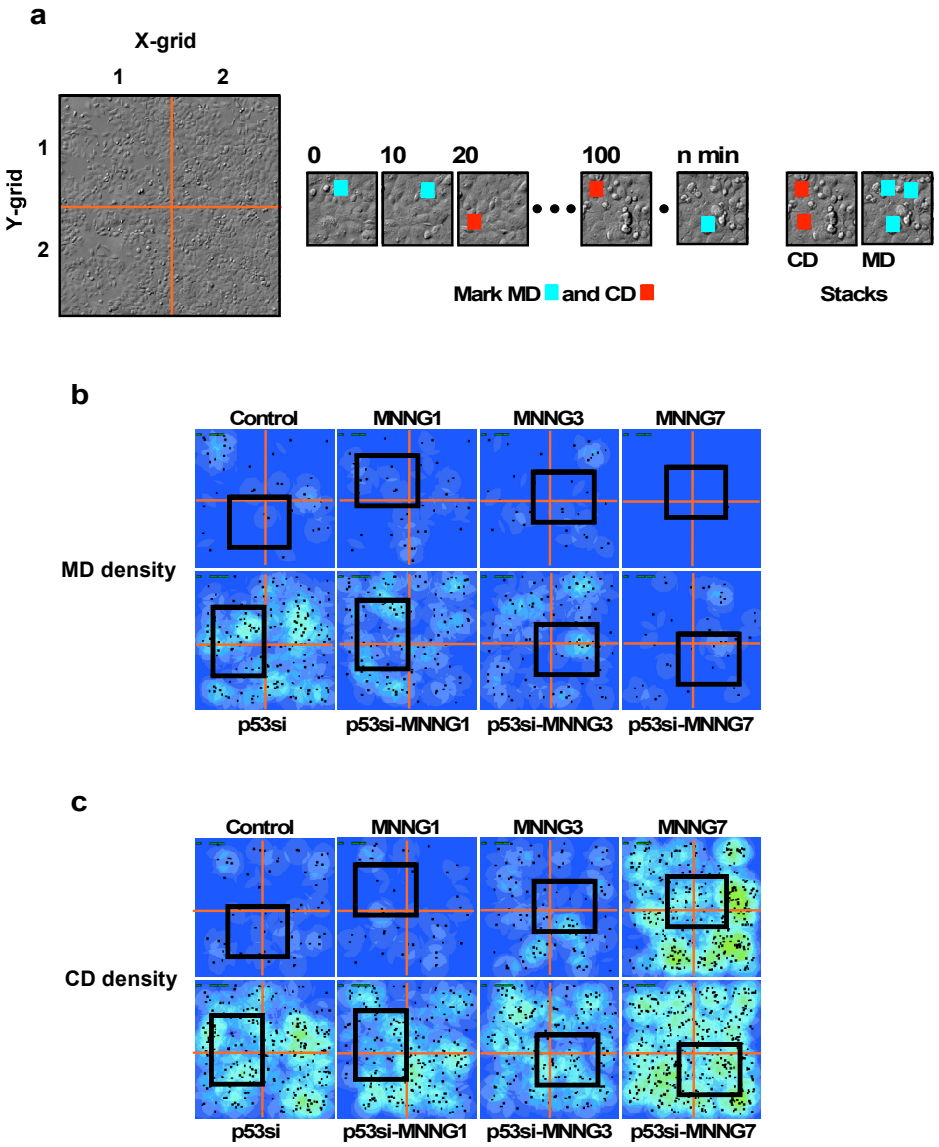

Supplementary Figure 6. Counting MD and CD using live-cell imaging videos. (**a**) Each time point of the video image was divided into four squares, and CD and MD events in each square were marked to determine the overall numbers of events that occurred during imaging. Three independently generated videos were used, and 12 squares were thus counted. The positions of MD and CD events were also stacked to generate MD and CD density maps. MD (**b**) and CD (**c**) density maps were created using a similar approach to cell density determination (see Fig. S2b). Density was shown using a heat map scale. Black squares correspond to the area used for single-cell tracking.

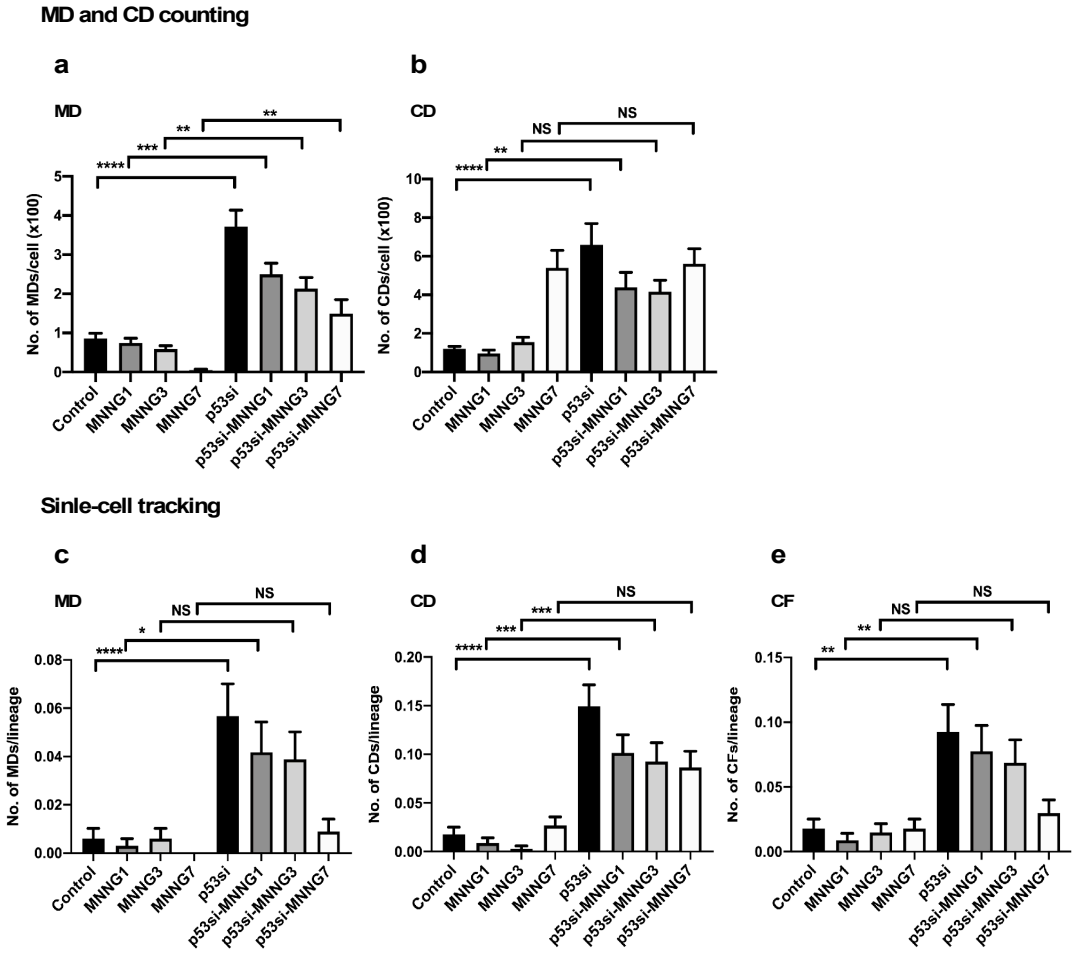

Figure 4. Analysis of MD, CD, and CF using counting and single-cell tracking analysis. Control and p53si cells were exposed to 1, 3, and 7 µM MNNG to produce Control and MNNG1, MNNG3, and MNNG7 cells, and p53si and p53si-MNNG1, p53si-MNNG3, and p53si-MNNG7 cells, respectively. The numbers of MD (**a**) and CD (**b**) events that occurred during the tracking time (4,000 min) were determined by counting. Three independently generated videos were used and counting was thus performed (see Fig. S6a) in 12 squares. The numbers of MD (**c**), CD (**d**), and CF (**e**) events that occurred during the tracking time (4,000 min) were determined using a cell-lineage database. The numbers of MD, CD, and CF events in each cell lineage were determined (n=335). (**a-e**) Statistical analysis was performed by ordinary one-way ANOVA (Tukey's). NS: non-significant, *P < 0.05, **P < 0.01, ***P < 0.001, ****P < 0.0001. Standard errors are shown.

In silico generation of cell-lineage database of p53si cells

Although CDs were found in p53si cells at 0.125 events per 10 min/300 lineages, the occurrence of CD during expansion of the p53-silenced cell population would act to counteract the expansion. To determine if the induction of CD did indeed have such an impact, we generated an *in silico* cell-lineage database assuming that CD did not occur (Fig. 5a). Cell-lineage data terminated by CD were replaced with cell-lineage data for its sibling, if the sibling continued to grow. The cell population expansion

rate of the *in silico*-generated cells (p53si-Sil(-CD) cells) (Fig. 5b) showed that CD occurring in p53si cells caused a 7.4% reduction in the cell population size at a tracking time of 4,000 min (Fig. 5b; p53si vs. p53si-Sil(-CD) cells). The estimated cell population size of the p53si-Sil(-CD) cells was larger than that of the Control cells and the *in silico*-generated Control cells (Control-Sil(-CD) cells), implying that the expansion curve of the p53si cell population does not represent its reproductive ability due to the occurrence of CD. Indeed, these results suggest that p53si cells have a higher population growth ability than Control cells (Fig. 5b). We therefore concluded that p53 silencing *per se* promotes cell proliferation, and the reduced cell population expansion in p53si cells is due to CD.

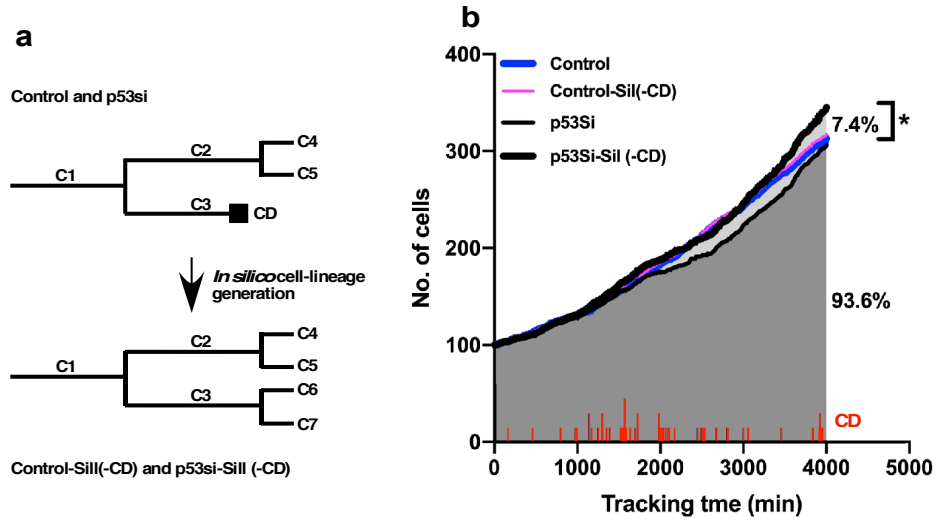

Figure 5 *In silico* generation of cell-lineage database. (**a**) In silico generation of cell-lineage database. In silico generation of cell-lineage database for the evaluation of the impact of CD on the population expansion. If the growth of a cell was terminated by CD, e.g. C3, the corresponding cell-lineage data were replaced with cell-lineage data for its sibling (C2) in silico, creating cells C6 and C7. (**b**) A cell population expansion curve was generated using the in silico-created cell-lineage database for Control and p53si cells (Control-Sil(-CD) and p53si-Sil(-CD), respectively). At a tracking time of 4,000 min, CD resulted in a 7.4% reduction in the population size of p53si cells. The frequency of CD (red lines) occurring during tracking is also shown. Statistical analysis was performed by ordinary one-way ANOVA (Tukey's). *P < 0.05.

Events leading to MD

MD and CF could have a greater impact than CD in terms of creating diversity in the cell population by causing the formation of aneuploid cells [27-32], if progeny produced by MD or fused cells survive. We

therefore focused on MD and CF (Fig. 6) by examining the relationships between these events. We investigated how normal growth patterns involving BD were shifted to MD, by analyzing cellular events that occurred prior to MD. We identified MD in the videos and traced the cell-lineages back to identify the preceding events. We identified two patterns: MD occurring in progeny produced by BD and in progeny fused with another cell (Fig. 6a). Interestingly, the pattern where CF occurred prior to MD was dominant in both Control and p53si cells (CF➛MD). Notably, p53 silencing induced MD through CF➛MD. We further analyzed the process leading to MD by searching for the origin of cells that underwent CF by tracing back the fused cells (Fig. 6b), and found that most CF events occurred between siblings produced by BD. The p53 silencing thus mainly promoted the sequence of events BD, CF of BD siblings, followed by MD (BD➛CF-sibling➛MD). We then examined the fate of the progeny of MD. Although the progeny of MD have been reported to be fragile, some are capable of entering a growing cycle [29, 30]. Indeed, we found that 3.5 to 3.8% of progeny produced by MD underwent BD (Fig. 6c). When the number of such progeny was compared between Control and p53si cells, the chance of producing progeny that underwent BD after MD was increased 14-fold by p53 silencing (0.7 progeny of MD/100 cell lineage of p53si cells vs. 0.05 progeny of MD/100 cell lineages of Control cells), suggesting that p53 silencing promotes the sequence of events, BD➛CF-siblings➛MD➛progeny-BD.

The induction of this sequence of events could be counteracted by MNNG, and the number of MD was reduced by MNNG in a dose-dependent manner (Fig. 4a and c). Indeed, plots of the numbers of MDs against the numbers of BDs in p53si and p53si-MNNG1, p53si-MNNG3, and p53si-MNNG7 cells showed direct proportionality (Fig. 6d), suggesting that MNNG suppresses BD and consequently inhibits the events BD➛CF-siblings➛MD➛progeny-BD.

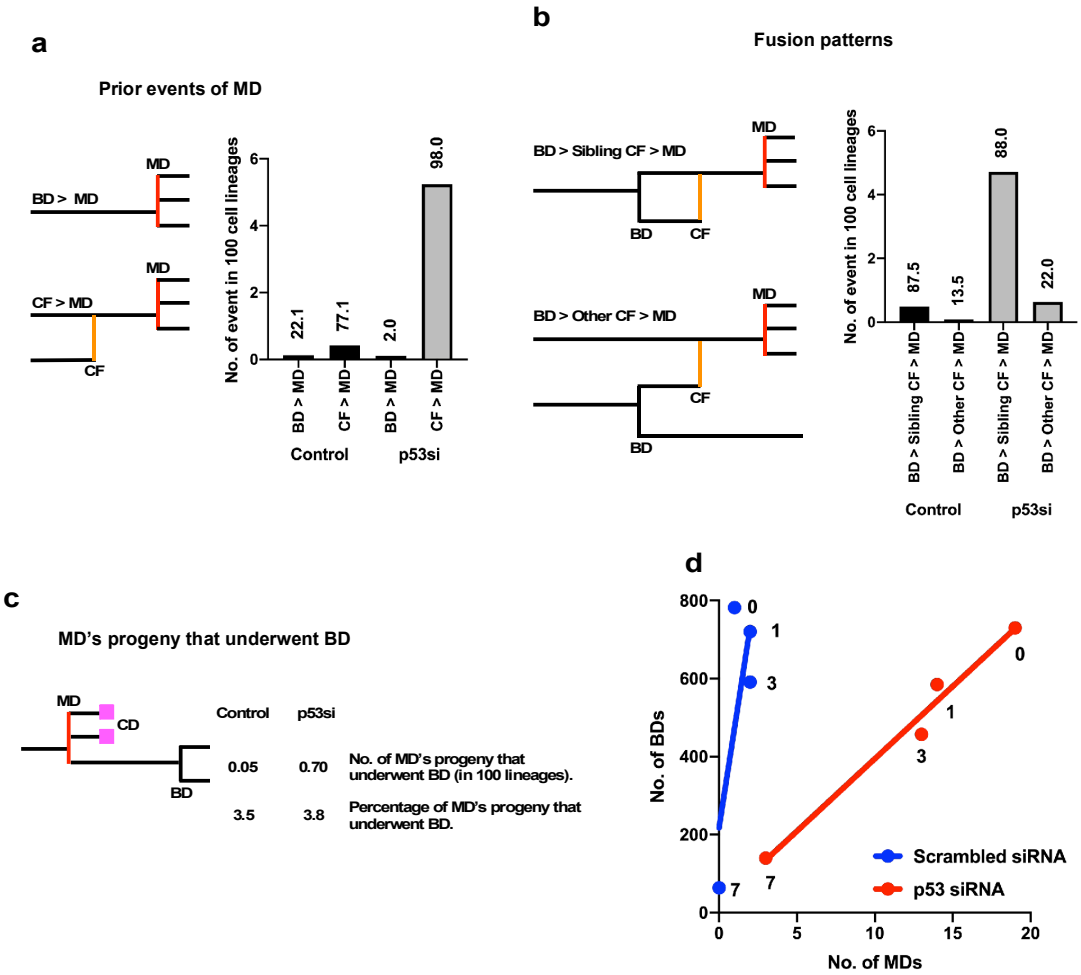

Figure 6. Events leading to the induction of MD. (**a**) Cellular events that occurred prior to MD were analyzed by tracing cell-lineages backwards. (**b**) Cells that underwent CF were determined by tracing cell-lineages backwards. (**c**) Progeny produced by MD were tracked and the number of progeny that underwent BD was determined. (**d**) The number of MD events was plotted against the number of BD events. Numbers in (**d**) indicate the doses of MNNG.

Cell-fate simulation algorithm

The above data suggest that the fate of the progeny of p53-silenced cells could affect the characteristics of the resulting cell population. However, it was difficult to follow the fate of individual cells by monitoring live cells, because the culture eventually became over-confluent. To overcome this limitation and further analyze the effects of p53 silencing on the characteristics of the cell population, we developed a cell-fate simulation algorithm using information in the cell-lineage database (Fig. S7, see Experimental procedures). The algorithm can perform five different modes of simulations depending on the settings for simulation time and number of progenitors, corresponding to the number

of cell-lineage datasets. The simulation was carried out as follows: generating Source data containing the categorized information of events, converting the Source data into Simulation arrays to assign a length of time to an event (Evt) and an event type, and creating a cell-lineage database. Among the five simulation modes, Standard mode (Std) was performed using one Source data, Intermediate mode (Ind) was carried out using virtual Source data created by other Source data, Mixed culture mode (MX) used two Source data to perform simulations of two different types of cells in one cell population, Standard-Sequential mode (SS) was used for virtual drug treatment, and Mixed culture-Sequential mode (MCS) was a MX mode-version of Sequential simulation. An example cell-lineage maps generated by empirical single-cell tracking analysis and the algorithm are shown in Fig. S8a and b, respectively (cell lineage maps generated by the algorithm were deposited in Dryad).

.

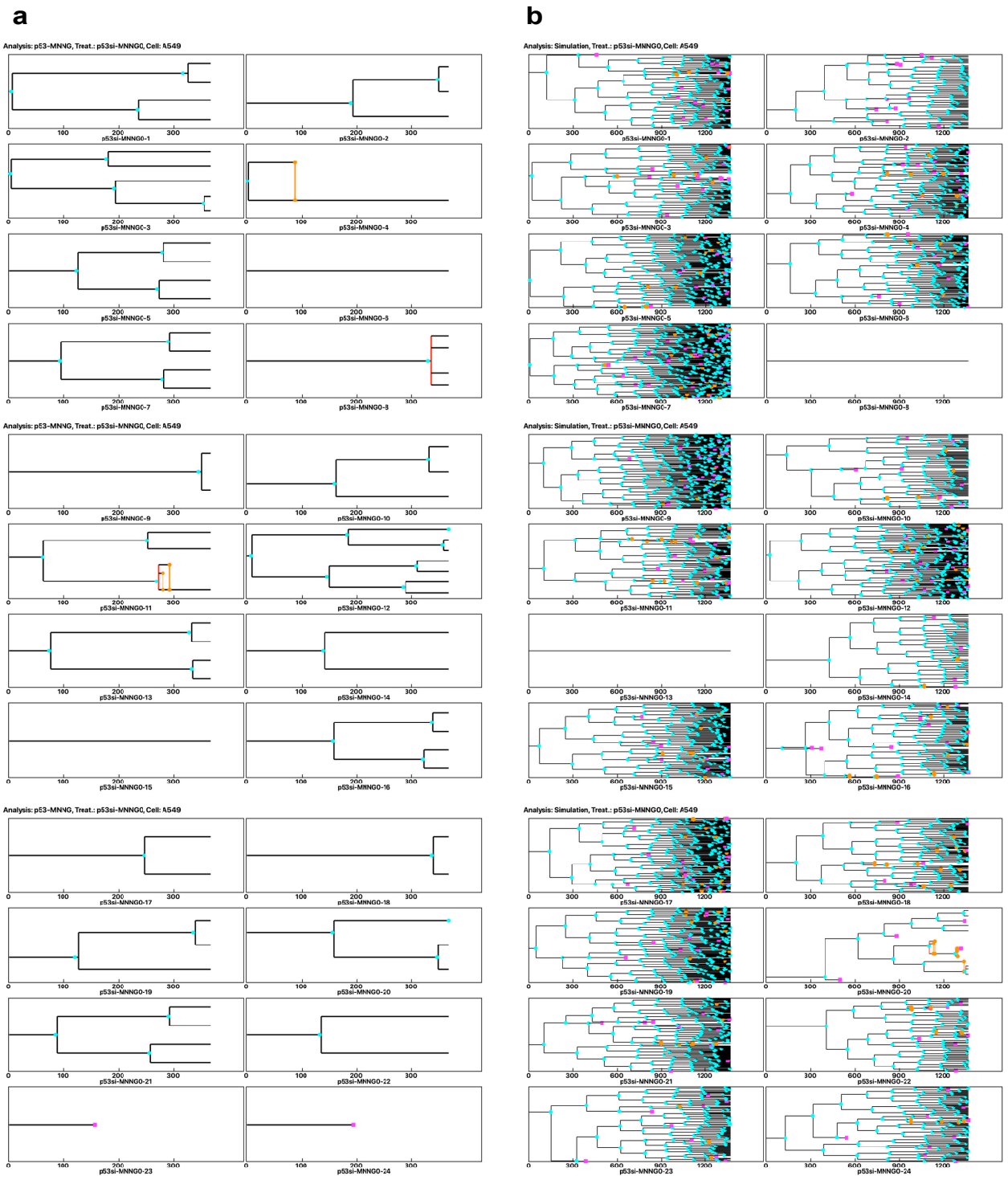

Supplementary Figure 8. Cell-lineage maps generated by single-cell tracking and a cell-fate simulation algorithm. (**a**) Cell-lineage maps generated by cell-lineage database Control cells. The single-cell tracking analysis created 335 cell-lineage datasets, and 16 cell-lineage maps are shown. (**b**) Cell-lineage maps generated by simulation using source data-p53si. The simulation created 2,500–5,000 virtual cell-lineage datasets, and 16 cell-lineage maps generated from the virtually created cell-lineage datasets are shown. Light blue circle, mitosis; pink square, CD; orange circle and orange vertical line, CF; black vertical line, BD; red vertical line, MD.

Number of progenitors used for simulation

We characterized the algorithm by performing a series of test simulations. We first performed simulations with 300, 500, 1,000, 1,500, and 2,000 progenitors with a simulation time of 15,000 min, repeated five times to detect variations in the simulation. Cell population expansion curves of virtually created Control cells (Control-Sim cells) are shown in Fig. S9a. Under these conditions, the variation was <2% of the average number of cells when the simulation was carried out with >1,000 progenitors. The simulation performed using the Source data-MNNG7 (Fig. S9b) produced a larger variation, but this converged to about 6% when the simulation was carried out with >1,000 progenitors. We therefore performed the simulation with 1,000–2,000 progenitors and repeated the simulation five to 10 times (total of 5,000–10,000 progenitors).

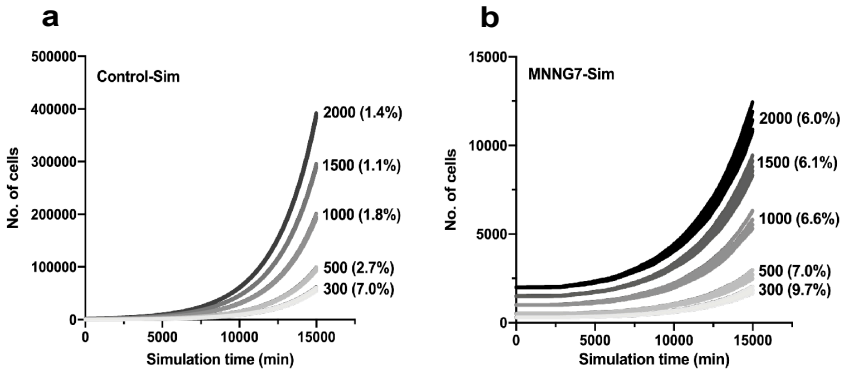

Supplementary Figure 9. Determination of number of progenitors required to perform a reproducible simulation. The simulation was performed with 300–2,000 progenitors using either the Source data-Control (**a**) or Source data-MNNG7 (**b**). Each simulation was repeated five times and virtual cell-lineage databases for Control-Sim and MNNG7-Sim cells were created to determine the population expansion curves of the virtual cells. The percentage of variation relative to the average at simulation time 15,000 min is also shown.

Simulation of cell population expansion and comparison between virtual population expansion curves created by simulation and empirical curves determined by single-cell tracking

We then evaluated the accuracy of the simulation by referencing the cell population expansion curves determined by empirical single-cell tracking analysis (Fig. 7). In the simulations, we used Std mode with Source data generated from the cell-lineage database for Control, MNNG1, MNNG 3, and MNNG 7, p53si, p53si-MNNG1, p53si-MNNG3, and p53si-MNNG7 cells, and performed each simulation

with 5,000 progenitors for 15,000 min. The number of progenitors was normalized to 100 to compare the results obtained by simulation with those obtained by single-cell tracking analysis. During the simulation with the Source data-Control, the virtual cell population size increased 193.5-fold (5,000 to 967,281 cells), and about 2×10^6 virtual cells were created in the simulation period of 15,000 min. The growth curves generated by the simulation using Source data-Control and Source data-MNNG1, MNNG3, and MNNG7 (Fig. 7a, 0–4,000 min) were consistent with the curves determined using single-cell tracking analysis (Fig. 2g), although the Control-Sim cell curve intersected with the MNNG1-Sim cell curve at a simulation time of about 10,000 min (Fig. 7b, 0–15,000 min). To evaluate the accuracy of the simulation, we calculated the average percent difference between the cell numbers determined by the simulation and by empirical single-cell tracking analysis (Fig. 7c-f). When the number of cells determined by single-cell tracking was calculated as 100%, the average difference was 1%–6%. We then performed a similar analysis with the Source data-p53si and Source data-p53si-MNNG1, p53si-MNNG3, and p53si-MNNG7. Cell population expansion curves determined using these Source data also showed consistent patterns (Fig. 7g, 0–4,000 min, and Fig. 7h, 0–15,000 min) with those determined by single-cell tracking analysis (Fig. 2h). The percent differences were within 0–8% (Fig. 7i-l). We thus concluded that the simulation could be performed within a variation of maximal 8% compared to the results of empirical single-cell tracking.

The results of the simulation performed using Source data created from an *in silico*-generated cell-lineage database (p53si-Sil(-CD); Fig. 5b) are shown in Fig. 7h. At a simulation time of 15,000 min, the number of p53si-Sil(-CD)-Sim cells was 1.7-fold higher than that of p53si-Sim cells, again confirming that the population expansion of p53si cells was hindered by the occurrence of CD.

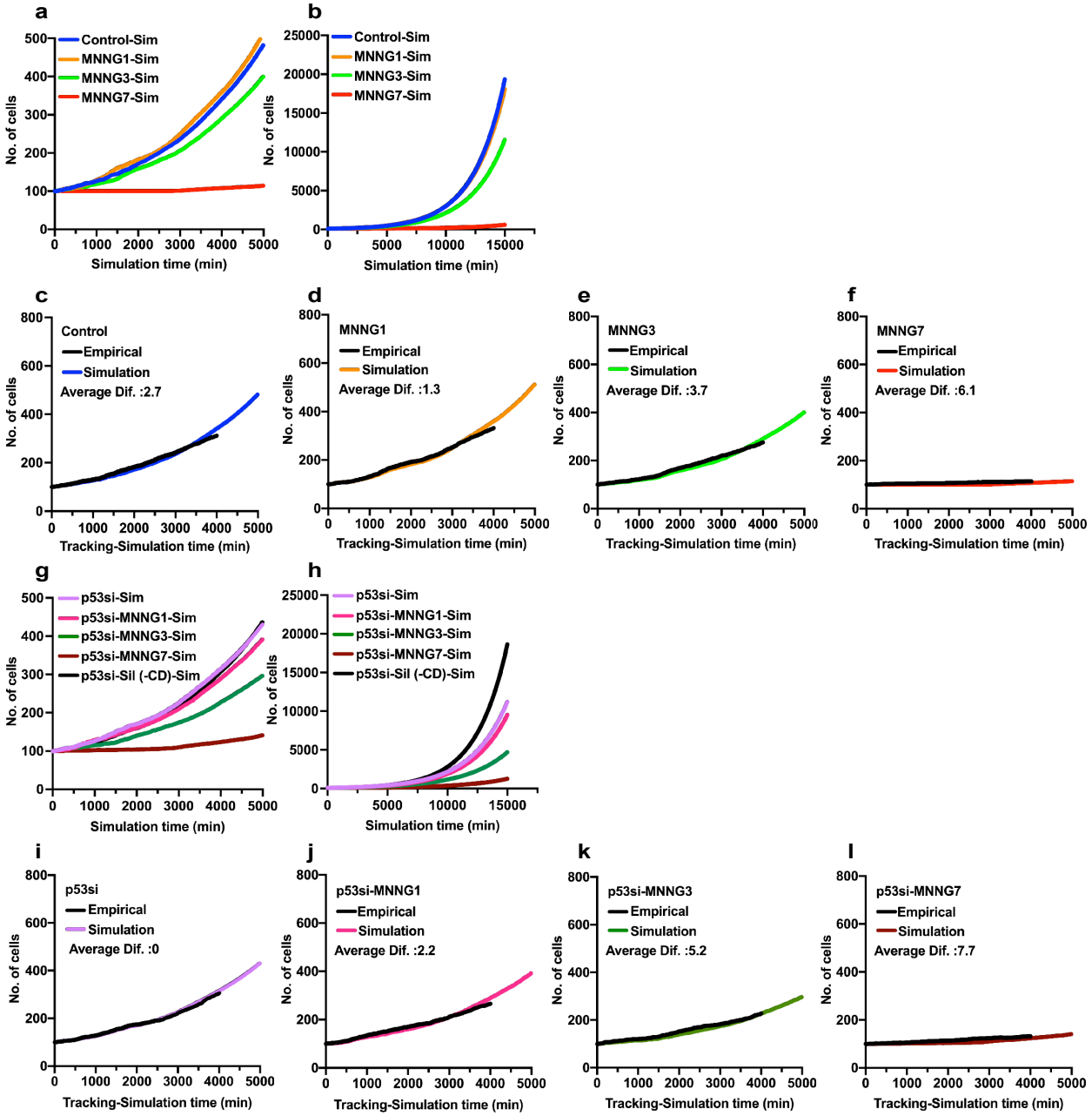

Figure 7. Simulations of effects of p53 silencing and MNNG exposure on cell population expansion. Simulations were performed using Source data generated from cell-lineage data, Control, and MNNG1, MNNG3, and MNNG7, and p53si, and p53si-MNNG1, p53si-MNNG3, and p53si-MNNG7 with a total of 5,000 virtual progenitors for a simulation time of 15,000 min. (**a** and **b**) Virtual cell population expansion curves of Control-Sim cells and cells exposed to various doses of MNNG (**a**: 0–4,000 min, and **b**: whole scale, 0–15,000 min). (**c**, **d**, **e**, and **f**) Data obtained from the simulation were compared with growth curves determined by empirical single-cell tracking analysis; (**c**) Control, (**d**) MNNG1, (**e**) MNNG3, and (**f**) MNNG7). 15,000 min). Difference (%) was determined by obtaining the sum of the number of Empirical cells/the number of Simulated cells determined at each simulation time point divided by 1,500 simulation time x 100. For example, a difference of 2.7% implied that the simulation generated 2.7% more cells compared with the Empirical data. (**g** and **h**) Virtual cell growth curves of p53si-Sim cells and cells exposed to various doses of MNNG (**g**: 0–4,000 min, and **h**: whole scale, 0–15,000 min). (**i**, **j**, **k**, and **l**) These simulation data were compared with the cell population expansion curves determined by empirical single-cell tracking analysis; (**i**) p53si, (**j**) p53si-MNNG1, (**k**) p53si-MNNG3, and (**l**) p53si-MNNG7). Results of simulation obtained using Source data-p53si-Sil(-CD) were also included in **g** and **h**.

Doubling time of cells generated by the simulation

We also analyzed the doubling time of individual cells generated by the simulation, using the doubling time distributions of Control and MNNG1, MNNG3, and MNNG7 cells determined by single-cell tracking analysis as a reference (Fig. S10a-d, respectively). The average cell doubling time was prolonged following the increased dose of MNNG (31.23 to 41.85 h). The doubling time of individual cells generated by the simulation (Fig. S10e-h for Control-Sim, and MNNG1-Sim, MNNG3-Sim, and MNNG7-Sim cells, respectively) was similarly prolonged following the increase dose of MNNG (29.36 to 39.43 h), suggesting that the algorithm could simulate the effect of MNNG on cell doubling. Similarly, the effect of MNNG treatment on the cell doubling time of p53-silenced cells (Fig. S10i-l) could also be simulated using the corresponding Source data (Fig. S10m-p). On the other hand, the simulation tended to yield an average cell doubling time about 2 h shorter than that determined by single-cell tracking analysis. Given that the algorithm assigned a cell doubling time to each cell by generating a random number with arrays including data for cell doubling times, a long cell doubling time, e.g. 3,000 min, which occurred less frequently, may be less likely to be assigned, resulting in the generation of a virtual cell population with a cell-doubling time about 2 h shorter than that of cells analyzed by single-cell tracking. This shorter average cell doubling time could translate into an increased rate of cell population expansion, and the maximal 8% variation in cell growth curves (Fig. 7) could reflect the cell doubling time of the virtual cell population.

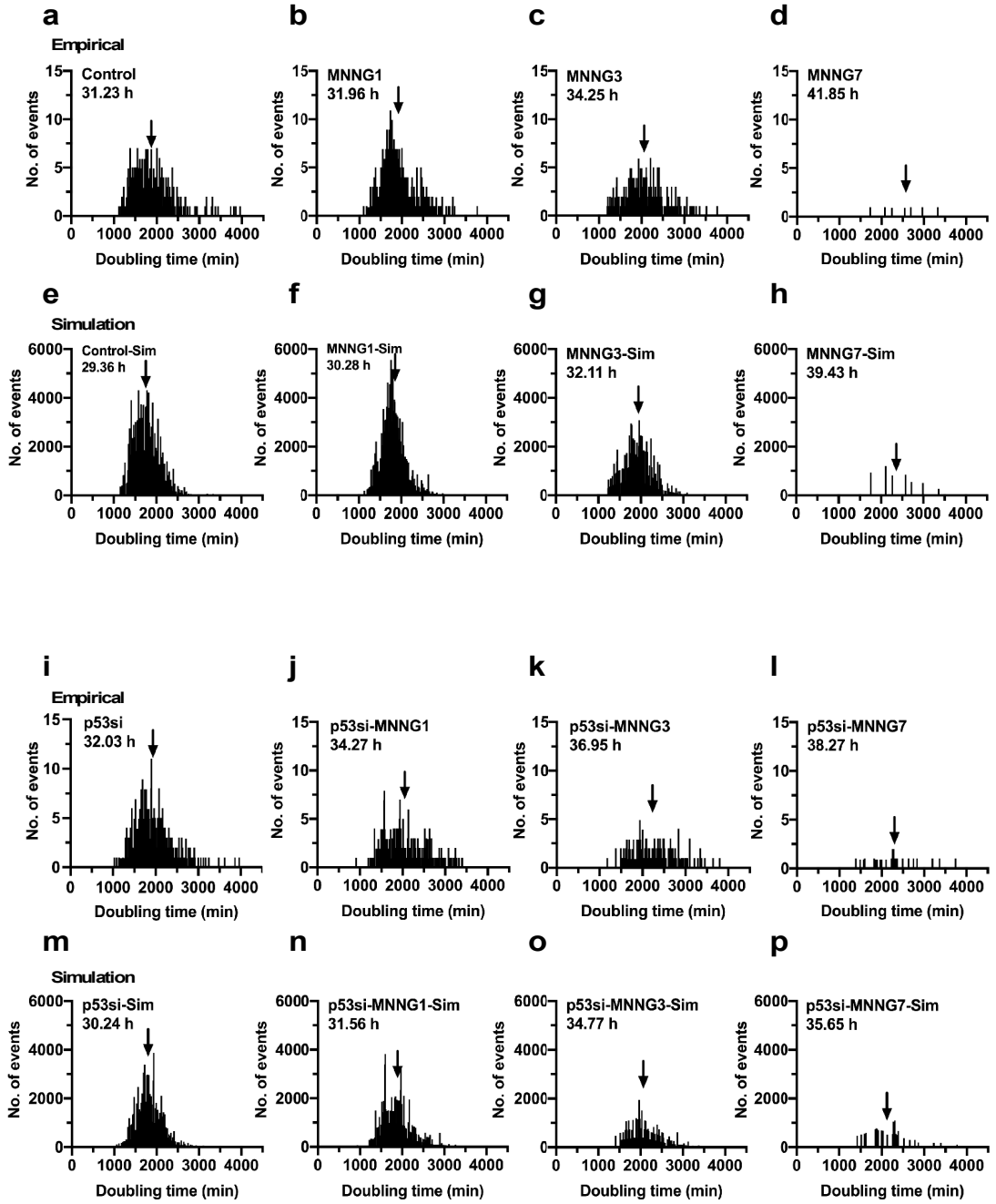

Supplementary Figure 10. Cell-doubling time distribution. Cell-doubling time distribution was determined using the cell-linage database (Empirical) and simulation (Simulation) data. (**a**, **b**, **c**, and **d**) Cell doubling times (Empirical) of (**a**) Control, (**b**) MNNG1, (**c**) MNNG3, and (**d**) MNNG7. (**e**, **f**, **g** and **h**) Simulations were performed using the source (**e**) data-Control, (**f**) MNNG1, (**g**) MNNG3, and (**h**) MNNG7, and the cell-doubling times of the virtual cells generated by the simulations are displayed. (**i**, **j**, **k**, and **l**) Cell doubling times (Empirical) of (**i**) p53si, (**j**) p53si-MNNG1, (**k**) p53si-MNNG3, and (**l**) p53si-MNNG7. (**m**, **n**, **o**, and **p**) Results of corresponding simulations are shown; the source (**m**) data-p53, (**n**) p53-MNNG1, (**o**) p53-MNNG3, and (**p**) p53-MNNG7. Arrow indicates the average cell-doubling time.

Simulation of occurrence of aberrant cellular events

Finally, we examined how the algorithm simulated the occurrence of MD, CD, and CF. Because these events were less frequent than BD, simulations were performed 10 times with 1,000 progenitors (total 10,000 progenitors) for a simulation time of 15,000 min. We compared the numbers of these events generated by the simulation (Simulate) with those obtained by single-cell tracking analysis (Empirical) by determining the numbers of MD, CD, and CF events that were generated by the simulation within 4,000 min. These data were then shown as the percent of total number of cells. The simulate results for MD (Fig. S11a), CD (Fig. S11b), and CF (Fig. S11c) show similar tendency with the empirical results, and the differences between the Empirical and Simulate results were within 1%. We therefore concluded that the cell-fate simulation algorithm could perform virtual cell experiments with similar accuracy than empirical single-cell tracking analysis.

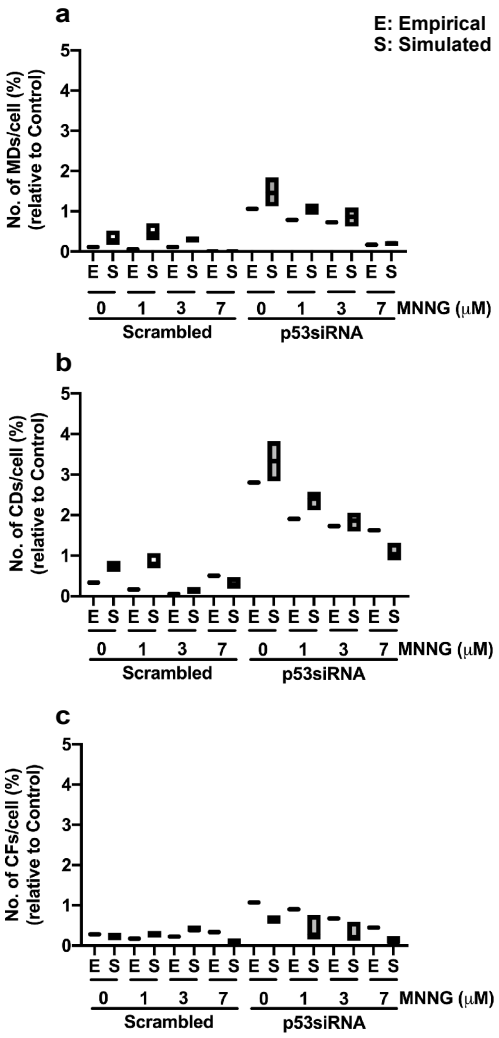

Supplementary Figure 11. Simulations of MD, CD, and CF. The numbers of MD (**a**), CD (**b**), and CF (**c**) events in a virtual cell population generated by the simulation (Simulation) were compared with those determined by single-cell tracking analysis (Empirical). The simulation was performed with 1,000 progenitors for a simulation time of 15,000 min and was repeated 10 times. The range of results obtained by the simulation is also indicated.

Virtual dose-response analysis and damage response

To begin the fate-simulation, we re-evaluated the responses of cells transfected with Scrambled siRNA or p53 siRNA to MNNG to generate virtual dose-response curves by creating Source data for every 0.5 μM of MNNG from 0–7 μM using Ind mode. The growth curves determined by the simulation are summarized in Fig. 8a and b, and the numbers of cells at simulation times of 4,000 and 15,000 min are shown in Fig. 8c and d, respectively. The dose-response curves of cells containing the low levels of p53 (p53-expressing cells) and p53-silenced cells determined at a simulation time of 4000 min showed

similar patterns to those determined empirically (Fig. 8c). Furthermore, p53-expressing cells showed stronger inhibition of population expansion in response to MNNG than p53-silenced cells at a simulation time of 15,000 min. These results suggest that the sensitivity of p53-silenced cells to MNNG was reduced by silencing. The sensitivity of p53-silenced cells to MNNG *per se* could thus be related to the direct cytotoxic effect of MNNG, and, in this context, the sensitivity of p53-expressing cells to MNNG could be dictated by both a direct effect and by induced damage responses following the accumulation of p53. To estimate the relative contributions of these two effects to the inhibition of cell-population expansion, we plotted the population expansion curves of Control-Sim, MNNG7-Sim, p53si-Sim, and p53si-MNNG7-Sim and determined the population-doubling time (Fig. 8e). We assumed that the difference in times between Control-Sim and MNNG7-Sim (7,150 min) was due to both the direct effect of MNNG and the damage response, while the difference between p53si-Sim and p53si-MNNG7-Sim (4,510 min) represented the direct effect of MNNG. Based on these data, we estimated that 63.1% and 36.9% of cell growth inhibition caused by 7μM MNNG exposure were due to the direct effect of MNNG and damage response, respectively.

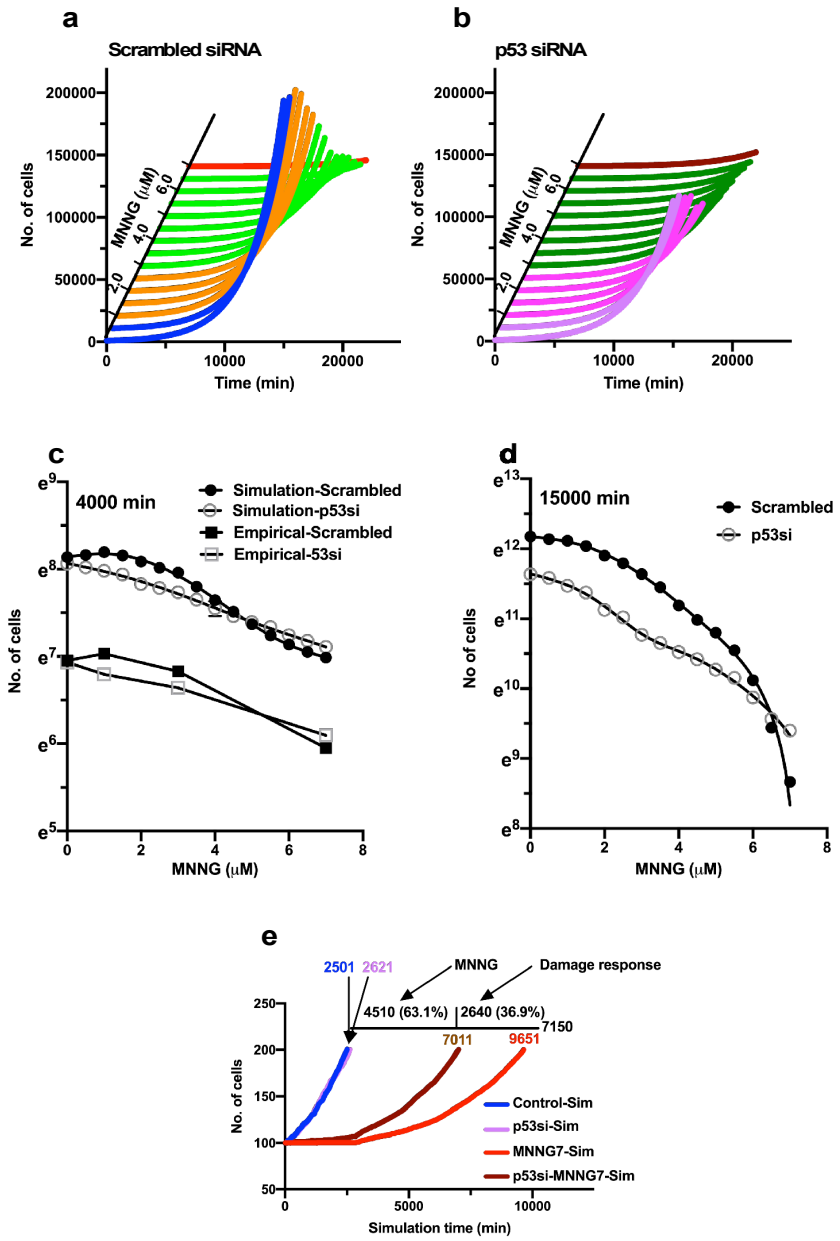

Figure 8. Virtual dose-response analysis and damage response. Virtual Source data corresponding to each 0.5 μM dose of MNNG was generated in Ind mode using Source data-Control, MNNG1, MNNG3, and MNNG7, p53si, p53si-MNNG1, p53si-MNNG3, and p53si-MNNG7. (**a**) Virtual cell growth curves generated by the simulation using Source data-Control to 1.5 (blue), 2–3 (orange), 3.5–6.5 (green), and 7 (red) are shown. (**b**) Virtual dose-response curves generated by the simulation using Source data-p53si to 1.5 (purple), 2–3 (pink), 3.5–6.5 (dark green), and 7 (marron) are shown. The numbers of cells at simulation times of 4,000 and 15,000 min were plotted on **c** and **d**, respectively. Standard deviations are shown. Results of single-cell tracking analysis are also indicated in **c**. (**e**) Time necessary to reach a cell population to be doubled (100 to 200 cells) was determined by Std mode using Source data-Control, MNNG7, p53si, and p53si-MNNG7. The difference in time between MNNG7-Sim (9,651 min) and Control-Sim (2,501 min) was 7,150 min. Similarly, the difference in doubling time between p53si-MNNG7-Sim and p53si-Sim was 4,510 min. Assuming that the difference in doubling time between MNNG7-Sim and Control-Sim represents the direct effect of MNNG and damage response, while that between p53si-MNNG7-Sim and p53si-Sim only represents the direct effect of MNNG, 63.1% and 36.9% of growth suppression in MNNG7-Sim were likely to be due to the direct effect of MNNG and the damage responses induced by the stabilization of p53, respectively.

Survival of the progeny of MD

Next, we asked how frequently the progeny of MD that can undergo BD can survive and grow by performing a simulation in Std mode with 2,500 progenitors for a simulation time of 20,000 min (13.8 days) instead of 15,000 min. The results of the simulation with 3.0–6.6 × 10^6 virtual cells are shown in Fig. 9. When the simulation was performed using the Source data-Control (Fig. 9a and b), no reproductive progeny produced by MD were detected. The computer animation (Movie S3 and Fig. 9c for still image at 20,000 min) visualizing the growth of the virtual cells showed only burgundy cells (progeny of MD; Fig. 9g, left) that eventually underwent CD or remained as non-growing cells. However, when the simulation was performed using Source data-p53si (Fig. 9d and e), some MD progeny underwent BD, accounting for 0.72% of the cell population at a simulation time of 20,000 min. The computer animation (Movie S4 and Fig. 9f for still image at 20,000 min) showed the expansion of green cells (MD progeny that underwent BD; Fig. 9g, right), in accordance with the suggestion [29, 30] that an aneuploid cell population could be generated by survival of the progeny of MD, promoted by p53 silencing.

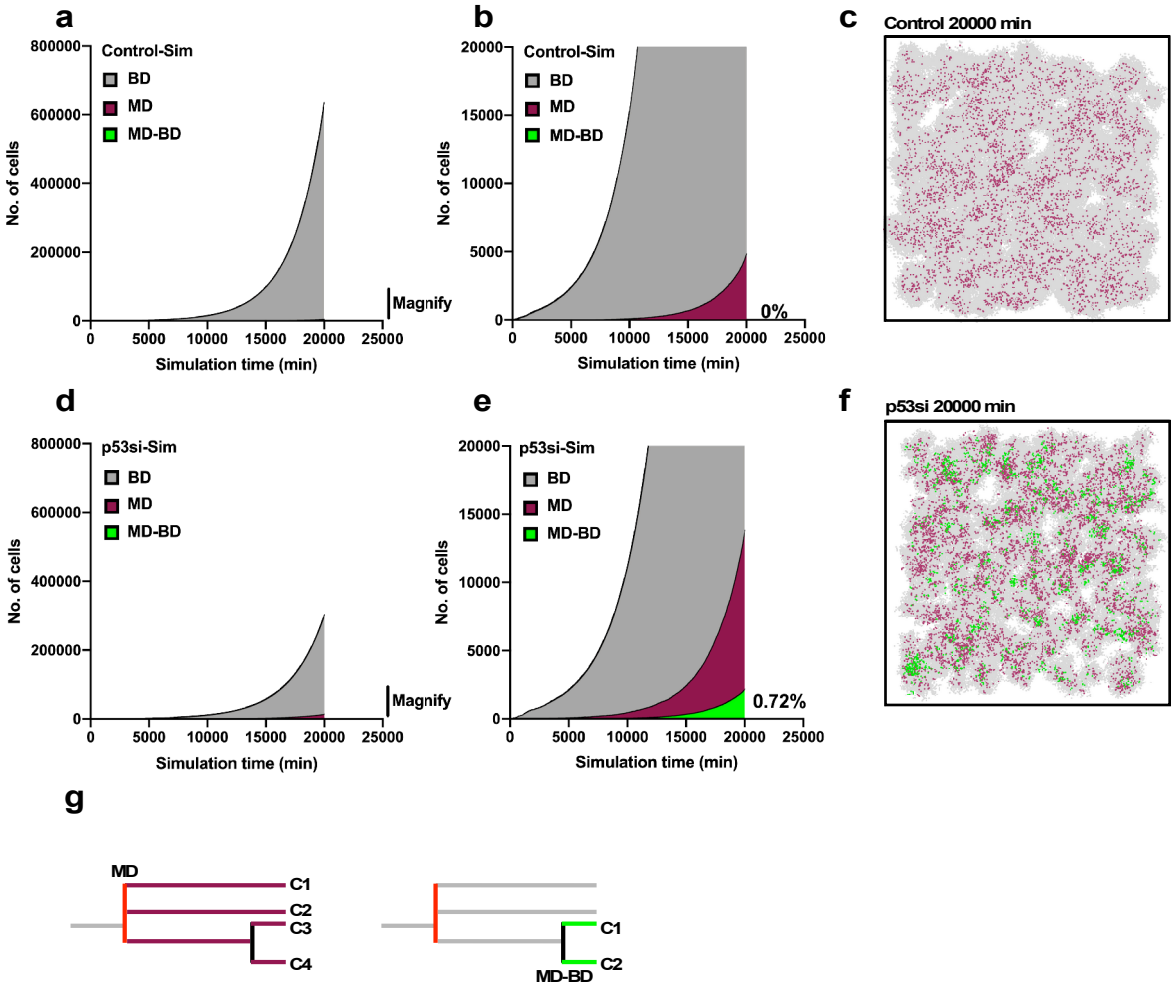

Figure 9. Simulation of growth of the progeny of MD. The simulation was performed using Source data-Control (**a-c**) and p53si (**d-f**) in Std mode. (**g**) The progeny of MD and those that underwent BD were indicated in burgundy and green, respectively. All other progeny were shown as gray. The simulation was carried out for 2,500 progeny, which generated 6.6 x 10^6 cells during the 20,000 min of simulation. (**a** and **b**) Whole-scale and magnified images generated by the simulation using the Source data-Control are shown in **a** and **b**, respectively. An animation was created to visualize the growth of the cells (Movie S4) and an image at simulation time 20,000 min is shown (**c**). (**d** and **e**) Whole-scale and magnified images generated by the simulation using Source data-p53si are shown in **d** and **e**, respectively. An animation was created to visualize the growth of the cells (Movie S5) and an image at simulation time 20,000 min is shown (**f**).

Limiting expansion of p53-silenced cells by p53-expressing cells

We then investigated the effect of p53-expressing cells on the growth of p53-silenced cells, given that p53-silenced cells likely arise within a p53-expressing cell population during tumorigenesis. We performed a simulation based on the assumption that p53-expressing and p53-silenced cells comprised 96% and 4% of the cell population, respectively, using MX mode with Source data-Control and p53si.

A total of 1.2×10^7 virtual cells were generated after 20,000 min of simulation, but the percentage of p53-silenced cells was reduced to 2.4% (Fig. 10a) because of the frequent occurrence of MD, CF, and CD (Fig. 10b). The p53-expressingd cells are shown as blue cells in the computer animation (Movie S5 and Fig. 10c and d for still image at 20,000 min). These data suggested that, although p53-silenced cells generated diversity in their cell population, p53-expressing cells suppressed the expansion of p53-silenced cells. We suggested that the occurrence of CD in p53-silenced cells is the main factor limiting the expansion of p53-silenced cells (Fig. 5b). Indeed, a simulation using Source data generated from p53si-Sil(-CD) showed that p53-expressing cells were unable to suppress the expansion of p53si-Sil(-CD)-Sim cells (Fig. 10e; 4.0% to 4.1%, and f), again suggesting that CD acts as a major factor limiting the population size of p53-silenced cells.

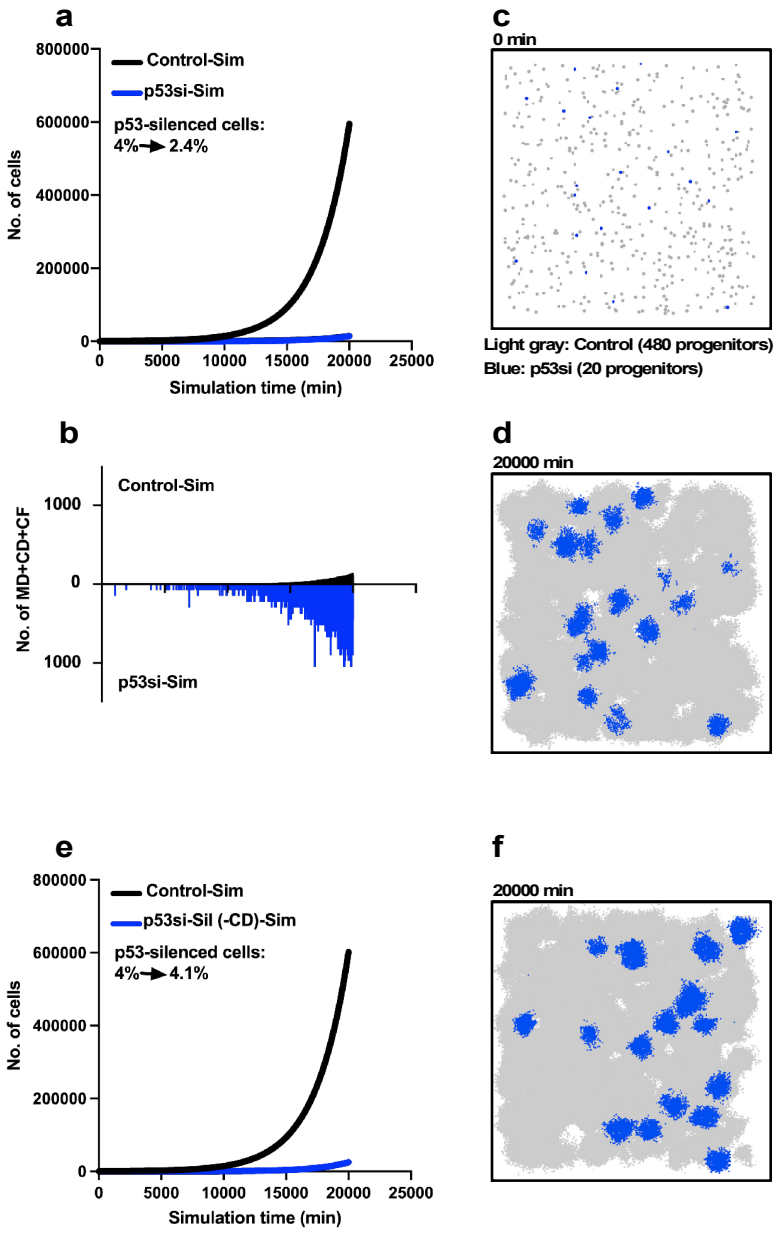

Figure 10. Limiting expansion of p53-silenced cells in a p53-expressing cell population. We simulated the expansion of the p53-silenced cell population (4% at the initial time point) in a p53-expressing cell population (96% at the initial time point) using MX mode with source data-Control and p53si for a simulation time of 20,000 min with 500 progenitors and repeating 10 simulations (total 5000 progenitors). (**a**) Simulation of 480 p53-expressing progenitors was carried out using Source data-Control and 20 p53-silenced progenitors with Source data-p53si. The initial percentage of p53-silenced cells was 4%, which was reduced to 2.4% at 20,000 min. (**b**) The sums of MD, CD, and CF events are shown. (**c** and **d**) Still images of the animation (Movie S6) at simulation times 0 and 20,000 min are also shown in **j** and **k**, respectively. (**e** and **f**) Simulation was performed using Source data-p53si-Sil(-CD) (**e**), and a still image of the animation at 20,000 min is shown (**f**). In the animation, p53-silenced cells are indicated in blue.

Damage response and its impact on p53-silenced cells by p53-expressing cells

The relative population-expansion rates of p53-expressing and p53-silenced cells were altered by exposure to MNNG (Fig. 7). We therefore simulated the responses of a cell population comprising p53-expressing (96%) and p53-silenced cells (4%) to virtual MNNG treatment using MCS mode. We used Source data-Control and p53si up to a simulation time of 9,900 min, and the Source data was then switched to the relevant virtual MNNG exposure and the simulation was continued for another 10,000 min (total 20,000 min simulation) (Fig. 11a). We simulated the responses of cells to 1.5, 3, 5, 6, and 7 μM MNNG using Source data-MNNG3 and MNNG7, and p53si-MNNG3 and p53si-MNNG7, and virtual Source data-MNNG1.5, MNNG5, MNNG6, and p53si-MNNG1.5, p53si-MNNG5, and p53si-MNNG6. In the computer animation, the brightness of the virtual cells was reduced at a simulation time of 10,000 min to highlight the virtual exposure (Movie S6 and Fig. 11a). The expansion of p53-silenced cells was still suppressed by p53-expressing cells following exposure to 1.5 and 3 μM MNNG (Fig. 11b-e). However, the suppression became less prominent at 5 μM MNNG (Fig. 11f and g), and p53-silenced cells started to expand their population over that of the p53-expressing cells at doses >6 μM MNNG (Fig. 11h-k). These results suggested that the damage responses induced in p53-expressing cells allowed the expansion of the p53-silenced cells (Fig. 11l). Indeed, if the exposure of cells to 7 μM MNNG was repeated four times, 93% of the cell population was replaced with p53-silenced cells (Fig. 11m).

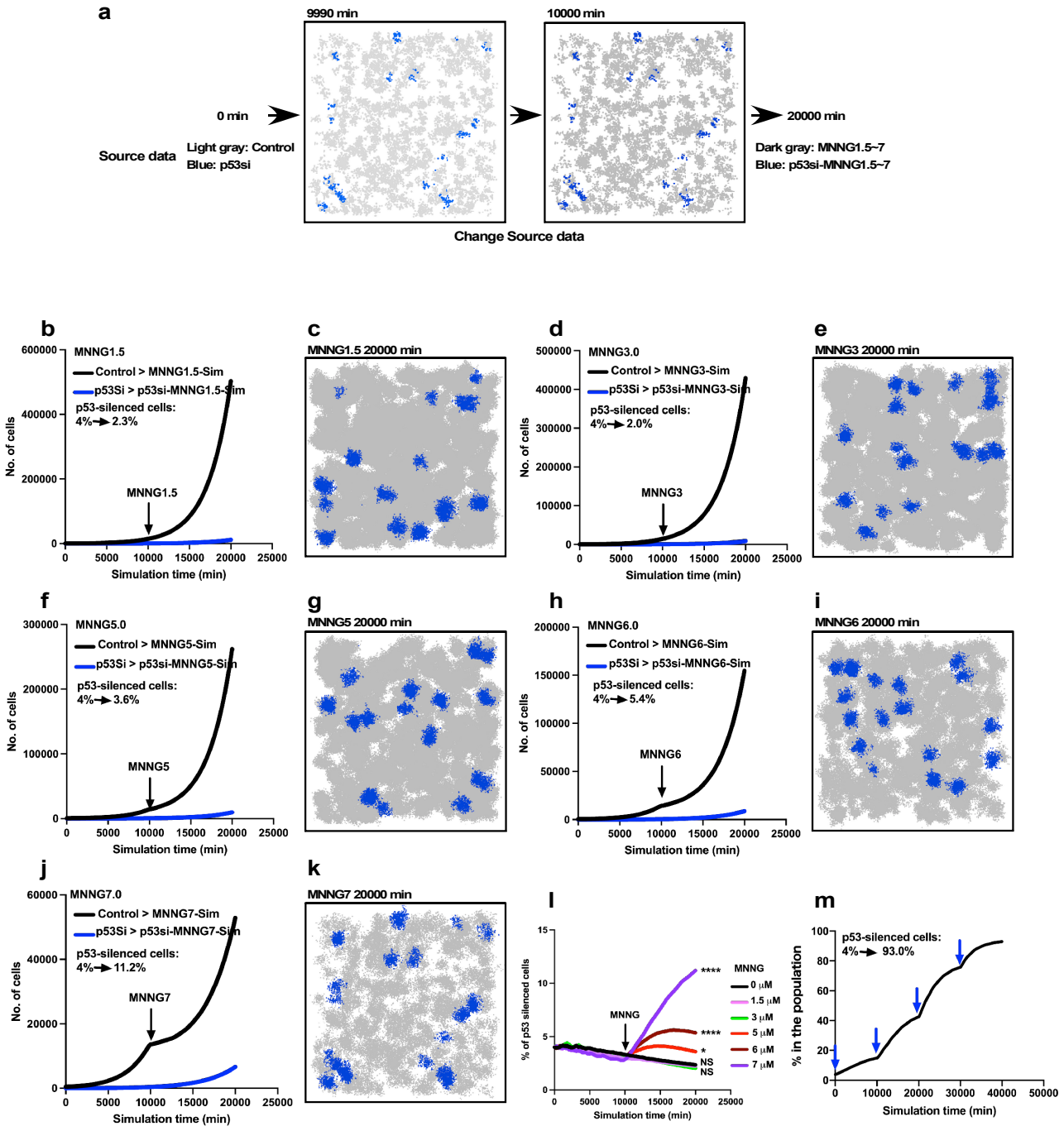

Figure 11. Expansion of p53-silenced cells in a p53-expressing cell population subjected to virtual MNNG exposure. We simulated the response of p53-silenced cells in a p53-expressing cell population to MNNG exposure using MCS mode. (**a**) The simulation was performed with 96% p53-expressing and 4% p53-silenced cells, using Source data-Control and p53si for 9900 min. The Source data was then switched to e.g. MNNG7 and p53si-MNNG7 for virtual MNNG treatment, and the simulation was continued up to 20,000 min. In the animation (Movie S7), the brightness of the image was changed to indicate the virtual MNNG treatment. (**b**, **d**, **f**, **h**, and **j**) In the simulation, virtual source data corresponding to (**b**) 1.5, (**d**) 3, (**f**) 5, (**h**) 6, and (**j**) 7 μM MNNG were created to perform a MNNG treatment. The numbers in the images indicate the percent of p53-silenced cells at simulation times 0 and 20,000 min. (**c**, **e**, **g**, **i**, and **k**) Still images from animations for (**c**) 1.5, (**e**) 3, (**g**) 5, (**i**) 6, and (**k**) 7 μM MNNG at 20,000 min are shown. (**l**) The percentages of p53-silenced cells in the population were plotted. Statistical analysis (n=10) was performed using data at simulation time 20,000 min by ordinary one-way ANOVA. NS: nonsignificant, *P < 0.05, ****P < 0.0001. (**m**) Based on the simulation data for 7 μM MNNG, percentage of p53-silenced cells following repeated 7 μM MNNG exposure was calculated. Arrows indicate the time that the virtual exposure was performed.

DISCUSSION

Stress-induced responses activated following the accumulation of p53 in a cell have been extensively studied, and the ways in which impairment of such responses may lead to tumor formation have been discussed [6-9]. For example, cellular senescence induced by oncogene stress can cause tumor suppression, and CD induced by exposure of the cells to a damaging agent could remove damaged cells that would otherwise have the potential to become cancer cells [7, 11-16]. On the other hand, some responses, e.g. DNA damage responses, may promote the survival of cells with gene mutations [7, 33]. Nevertheless, stress is an essential component activating the function of p53 to suppress tumor formation in this context. However, Valente et al. recently demonstrated that physiological oxygen tension induced p53-mediated regulation [34], implying that p53 exerts its tumor suppressor function under these conditions, which resemble physiological conditions, as supported by the current results for silencing the low levels of p53 retained in unstressed cells.

The characteristics of p53-expressing and p53-silenced cells are summarized in Fig. 12a. The growth of p53-expressing cells was maintained by strongly biasing their division to BD, and less frequently by the induction of other events, i.e. CD, MD, and CF. On the other hand, silencing of p53 led to frequent induction of CD in p53-silenced cells. Such CD appears to occur by a process distinct from damage-induced CD, and CD occurring in p53-silenced cells may be induced as a natural defense mechanism to remove cells lacking p53. Indeed, fate simulation in a population containing 4% p53-silenced and 96% p53-expressing cells demonstrated that expansion of the p53-silenced cells was suppressed by p53-expressing cells, and the induction of CD in p53-silenced cells hindered their expansion. After ~21 cell doublings of 500 progenitors including 4% of p53-silenced cells, the cell number increased to ~1×10^9, corresponding to ~1 cm of cancer tissue mass, while the relative content of p53-silenced cells was reduced to 1.2% (Fig. 12b). In this context, the expansion of p53-silenced cells with malignant potential was suppressed by p53-expressing cells, making p53-silenced cells effectively dormant cells. It has been proposed that metastatic cells are disseminated in the early stage

of tumorigenesis and then undergo dormancy [35, 36]. Those studies have tended to focus on the characteristics of metastatic dormant cells [37, 38], and further studies that focus on the cells surrounding metastatic cells may provide an insight regarding the dormancy, as observed with p53-silenced cells.

The p53-silenced cells were also characterized by the induction of CF (Fig. 12a), which can alter cell ploidy. In addition, CF increases the chance of the resulting cells undergoing MD to produce aneuploid cells. Interestingly, ploidy is frequently altered in malignant cancer cells harboring p53 with impaired function [39-43]. In addition, fibroblasts derived from $p53^{-/-}$ mice rapidly became tetraploid [11, 44], and loss of p53 function has been suggested to be essential for the survival of aneuploid cells [45-47]. A loss of cell cycle checkpoint control leads to aneuploid, polyploid, and tetraploid cells [48], and polyploid cells are thought to be produced as precursor cells that undergo MD through cytokinesis failure or mitotic slippage [39, 49, 50]. We observed CF following abscission and CF sometimes occurred between non-siblings. Cytokinesis failure or mitotic slippage may thus not be responsible for the observed CF, although the possibility of a persistent link between the fused cells cannot be ruled out [51]. Nevertheless, we demonstrated that silencing p53 in unstressed cells led to CF followed by MD. Furthermore, our simulation results suggest that the aneuploid progeny produced by MD can generate a cell population, implying the addition of genetic diversity to a cell population. As previously suggested [21], the ability of p53 to suppress tumor formation may be related to the normal growth of cells, and the formation may be related to non-mutagenic mechanisms of cancer development as exemplified by extrachromosomal DNA [52]. However, the addition of genetic diversity to a cell population *per se* may not be sufficient to overcome the cell population homeostasis barrier established by p53-expressing cells (Fig. 12b), and other events that trigger the expansion of p53-silenced cells may be required during tumorigenesis.

Induction of the damage response in p53-expressing cells could be one such event. Our simulation results suggested that 4% of p53-silenced cells in the p53-expressing cell population expanded to 11% following virtual exposure to 7 μM MNNG at a simulation time of 20,000 min (13.9 days). After repeating this exposure four times (40,000 min), the simulation revealed that p53-silenced cells

accounted for 93% of the cell population (Fig. 12b). The DNA damage response is supposed to suppress tumor formation, but in the current context, it could have a pro-malignant function. Whether p53 acts as a tumor suppressor can thus be largely influenced by the context of the cell population.

Given that cancer tissues are composed of heterogeneous cell populations, many different contexts may be involved in the process of tumorigenesis and we revealed one of the contexts using A549 p53 proficient lung carcinoma cells. Furthermore, the level of stress, e.g. DNA damage, caused by the cellular microenvironment could add another layer of complexity. To understand the process of tumorigenesis, these complexities need to be resolved. In this regard, cell-fate simulation algorithms could be used to resolve the complexity. Performing these simulations requires the creation of a cell-lineage database, and we estimated that the database generated by monitoring two cell divisions of 100 progenitors would be sufficient to simulate cell growth. Furthermore, because each cell line is likely to have unique growth characteristics and response patterns to treatment, once a cell-lineage database representing a specific growth characteristic or response pattern is archived, it can be used as a new public resource for cell biology and cancer research to predict and analyze the role of a cell in cancer development, and eventually to reveal the process of tumorigenesis.

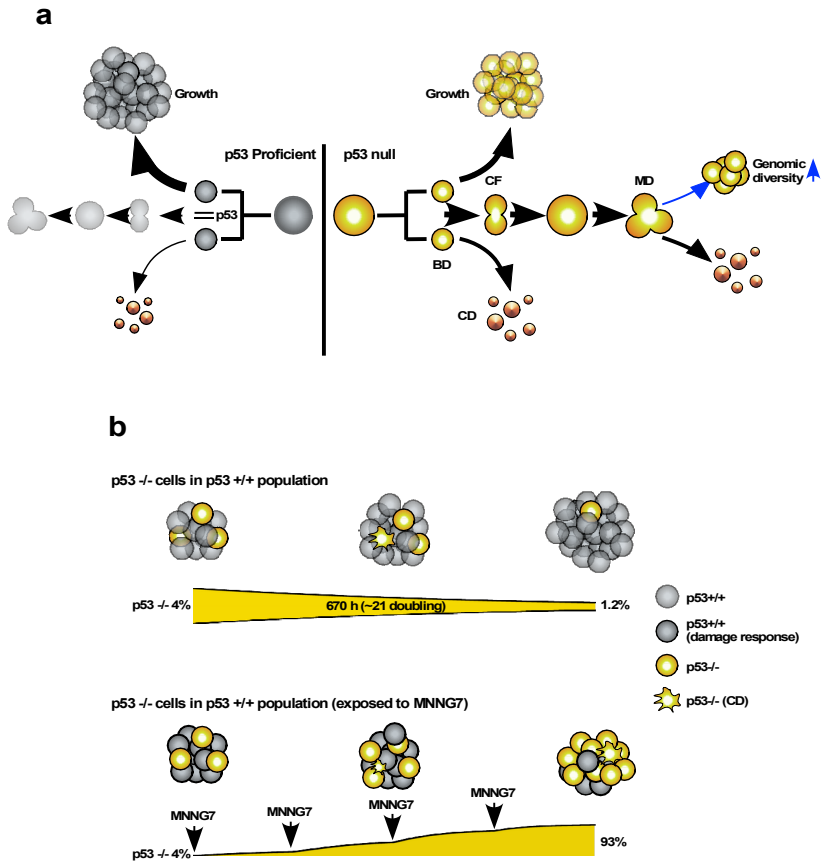

Figure 12. Role of the low level of p53 in maintaining the integrity of cells and damage response. (**a**) Characteristics of p53-expressing and p53-silenced cells. (**b**) Different fates of p53-silenced cells under unstressed and stressed conditions.

EXPERIMENTAL PROCEDURES

Cells and cell culture

A549-luc-C8 cells were purchased from Xenogen Corporation and cultured in RPMI containing 10% fetal bovine serum in a humidified atmosphere with 5% CO_2. Cells were plated in the center of each well of a cover glass Lab-Tek II 8-well chamber in 50 µL of cell suspension containing 3,500 cells and left to attach to the cover glass surface. Culture medium (0.75 mL) was then added to each well and the chamber was viewed under a microscope (Olympus IX81) after 24 h of plating.

Concurrent long-term live cell imaging, siRNA transfection, MNNG treatment, and single-cell tracking

Concurrent long-term live cell imaging and single-cell tracking were performed as described previously [53, 54]. Briefly, images were acquired under a microscope using near infrared DIC imaging with a ×20 dry objective (UPlanSApo, 20×/0.75 NA, α/0.17/FN2G.5) and a ×1.5 coupler (Quorum Technologies) to generate a ×30-equivalent image. Images were acquired by area scanning (5 × 5 dimension, 512 × 512 pixels each) using multi-dimensional acquisition mode in MetaMorph (Quorum Technology Inc, WaveFX, v7.8.12.0) with 34 ms exposure and XY piezo stage. Typically, 30 z-planes were acquired every 1 µm, and 512 × 512 pixel multi-layered .tiff files were created. Cells were maintained on the microscope stage in an environmental chamber (Live Cell Instrument, Korea) in a humidified atmosphere with 7.5% CO_2, and images were acquired every 10 min. Lipofection with scrambled siRNA and p53si RNA (Cell Signaling Technology) was performed approximately 24 h after cell plating using Effectene Transfection Reagent (Qiagen) with 1 µg siRNA in 742 µL transfection mixture, according to the supplier's instructions. Image acquisition was started immediately after siRNA transfection. At 24 h after siRNA treatment, cells were exposed to various doses of MNNG

(Sigma-Aldrich) for 30 min in serum-free RPMI, and the medium was then replaced with fresh RPMI containing 10% fetal bovine serum.

Acquired images were stitched (25 images covering 5 × 5 dimension, approximately 2500 x 2500 pixels) after selecting a focal plane from a multi-layered .tiff file, and the contrast of the stitched image was adjusted to generate a video sequence. We previously generated videos using commercially available software and freeware [53], but used in-house software in the current study to reduce the processing time [54]. To perform single-cell tracking analysis, each stitched image was segmented to determine the position of each cell [54]. Cell tracking was carried out by automatically chasing the segmented areas and by manual verification of the tracking results using in-house software [54]. During tracking, cellular events, i.e. BD, CD, MD, and CF, were identified, and a cell-lineage dataset was created. Each dataset included information on cell-lineage number, cell number, X and Y positions of cells, types of event occurring in the cell, link to its parent cell, and information on fused cells in the event of CF [54].

Western blotting

Cells were transfected with scrambled siRNA and p53siRNA and treated with various doses of MNNG after 24 h. At 48 h after treatment, the cells were harvested and proteins (15 μg) were separated by 10% sodium dodecyl sulfate-polyacrylamide gel electrophoresis. Western blotting was performed using anti-p53 antibody (1 μg/mL, DO-1; Invitrogen) and horseradish peroxidase-conjugated goat anti-mouse antibody (25,000-fold dilution; Abcam). Proteins were visualized using an ECL reagent (Pierce). Quantitation of p53 was performed using Image J.

Generation of density maps

To create a cell density map, we assigned a value of one to a pixel within the 20-pixel diameter area for cell density and 100-pixel diameter area for MD and CD density from the position of the cell or

position where MD or CD occurred. If an area overlapped with other areas, a pixel was assigned the sum of the number of overlapped areas. These values were used to generate heat maps.

Overall flow of the cell-fate simulation algorithm

The flow of the cell-fate simulation algorithm is shown in Fig. S7a. The simulation mode was selected from the available five modes (Fig. S7a, 1). Standard (Std) mode performed a simulation by setting a simulation time and an initial number of cells (progenitors) followed by Source data creation (Fig. S7a, 2, and Fig. S7b) or uploading, and generation of simulation arrays (Fig. S7a, 3, and Fig. S7b). Source data held the categorized information of events, and Simulation arrays (Fig. S7a, 3) were used to assign Evt and event type. Intermediate dose (Ind) mode was carried out by setting a simulation time, the initial number of cells, and an intermediate dose. Two sets of Source data were then generated or uploaded and virtual source data corresponding to the intermediate dose were created using those Source data. For example, if the intermediate dose was 5 μM MNNG, virtual source data were generated from Source data for 3 μM and 7 μM MNNG. Mixed culture (MX) mode performed a simulation for a virtual cell population composed of two cell types. A simulation time and initial numbers of the first and second cell populations were set. Two sets of Source data were used to simulate the growth of the first and second cell populations individually. Two sets of simulation arrays were also created. This mode could be used to simulate the growth of a cell population surrounded by another cell population. Standard-Sequential dose (SS) mode was used to perform virtual drug treatment. The simulation times before and after treatment, and the initial number of cells were set. Two sets of Source data for the first and second doses were used, and simulation arrays corresponding to each dose were created. Mixed culture-Sequential dose (MCS) dose mode was a combined version of MX and SS. This mode used four sets of Source data and generated four sets of simulation arrays. Initial processing was then performed by creating a Cell data information array (CDE) that included the Evt and event type assigned to each cell (Fig. S7a, 4, and Fig. S7d). Based on the information in the

CDE, a virtual cell-lineage database was created (Fig. S7a, 5, and Fig. S7e). After these initial processes, a repeated cycle of assigning Evt and event type (Fig. S7f), reassigning Evt and event type to adjust for the effect of CF on Evt (Fig. S7g), and creating a virtual cell-lineage database (Fig. S7h) were carried out until the simulation time was reached (Fig. S7a, 6). If SS or MCS mode was used, the cell-lineage database end was trimmed (Fig. S7i), Source data was switch to corresponding Source data, and the process proceeded to the second round of the repeated cycle (Fig. S7a, 7). When processing reached the simulation time, the simulation was terminated and the results were displayed.

Cell-fate simulation algorithm: Source data

Processing related to Source data, which comprised three types of data, is outlined in Fig. S7b. Source data were either uploaded or generated from a cell-lineage database. If the Source data were generated, information held in the cell-lineage database was converted into a Time dataset (Fig. S7b, 1), Event dataset (Fig. S7b, 2), and Recovery data (Fig. S7b, 3). The Time dataset held categorized Evt by event type, e.g. Evt between BD and CD (BD-CD data type) and Evt from time 0 min to the time that an event occurred in a progenitor (First event data type) (Fig. S7b, 1). The Event dataset contained the frequency of events, e.g. BD (BD data type), or BD that occurred following MD (BD-MD data type) (Fig. S7b, 2). Recovery was the percentage of cell lineages that underwent cell division at the end of single-cell tracking (Fig. S7b, 3). For example, if any of the progeny derived from a progenitor underwent BD within 20% of the single-cell tracking period, e.g. 320 to 400 min if tracking was performed for 400 min, this cell lineage was counted as one upon the calculation of the percentage. Thus, if 10 such cell lineages were found out of a total of 300, the recovery percent was 3.3%. Using Ind mode, virtual Source data were created from two sets of Source data using the formula: virtual Source data = Source 1+[(Source 2-Source1)/(Dose2-Dose1)]×(Intermediate dose-Dose 1) (Fig. S7b, 4).

Cell-fate simulation algorithm: Simulation arrays

The dataset stored in Source data was then converted into Simulation arrays that were used to assign Evt and event types (Fig. S7c). In the Source data, each categorized Time data was stored in the format, i.e. Evt, and the number of Evts that was found. For example, 20 min of Evt found four times was written as 20:4. In the simulation arrays corresponding to the Time dataset, this was converted to, e.g. 20, 20, 20, 20. If no corresponding type of event occurred, the array for the event held no data. To generate a simulation array for the Event dataset, the percentage of each event relative to the total number of cell divisions (total of BD and MD) was calculated. The maximum number of entries per array was 100. The total percentage of events could thus exceed 100, e.g. first event list (BD, CD, MD, and the number of cells with no cell division (nonDiv)). In this case, the percentage of each event was adjusted to make a total of 100. If the percentage of the event was <100, 0 was filled to make the total entry for the array 100. If no corresponding type of event occurred, an array for the event held no data. The Recovery percentage was calculated as described above.

Cell-fate simulation algorithm: Initial Evt and event-type assignment.

In the first event assignment (Fig. S7d), the CDE that held the status of each cell throughout a simulation was created. In this step, the cell-lineage number was generated following the initial number of cells set previously, and the cell number 0 was assigned to each progenitor. Using the FirstEvent array, Evt was then assigned to each cell. If the array was empty, the average time that BD occurred was calculated and -25% to +25% of the time selected by random number was assigned as Evt, and BD was then assigned to the cell. If the FirstEvent array held data, Evt was assigned by creating a random number, but if Evt was equal to the length of single-cell tracking, -30% to +30% of the length of the time of single-cell tracking was assigned as Evt and the event type was selected using the FirstEvent list array. If there was no entry in the array, NonDiv was assigned, otherwise, BD, MD, or CD was assigned. If CD was assigned, Evt was reassigned using the NonDivCD time data array.

Cell-fate simulation algorithm: Initial cell-lineage database creation

The cell-lineage database was created using information held by the CDE (Fig. S7e). This array contained information regarding Evt and event type as a blueprint of the virtual cells (Fig. S7e). If Evt exceeded the simulation time set previously, Evt was adjusted to a time equal to the simulation time, otherwise, a cell-lineage database was generated composed of an X position, Y position, time point, event type, cell-lineage number, cell number, parent cell information, cell number and the cell-lineage number of the cell that was fused in the event of CF. Because there was no information regarding the X and Y positions of the cells, these were filled as 0, but other data were created using the CDE. If the event type was BD or MD, information related to the progeny created by BD or MD was entered into the CDE following the generation of corresponding cell numbers for each progeny.

Cell-fate simulation algorithm: Evt and event-type assignment

In the repeated assignment cycle (Fig. S7a, 6), the next Evt and event type was determined based on the current event type. If the current event in a cell was NonDiv (Fig. S7f, 1), a randomized number between 0 and 100 was generated, and if the number was lower than the Recovery %, BD was assigned to the cell. In the next cycle, this cell was entered into a growing cycle. If the Evt was 80%–100% of the length of the single-cell tracking time, the Evt was determined by generating random numbers between 80 and 100. Assignment of BD in this manner only occurred once at the first cycle of the assignment. If the random value was higher than the Recovery %, either NonDiv or CD was assigned, in which case the % of CD of total cell division was calculated and, if the random number between 0 and 100 was lower than the CD%, a CD was assigned. In this case, Evt was assigned using the NonDivCD time array. If the random number between 0 and 100 was higher than the CD%, NonDiv was assigned, and the length of single-cell tracking time was assigned as Evt.

Next, if the current event was BD, information related to its sibling was searched for. If a sibling was found, either BD, MD, or CD was assigned using the BD list array, otherwise BD, MD, CF, or CD was assigned. If the event assigned by the BD list array was CF, then its sibling was again searched. If no sibling was found, Evt was assigned by the BDCF time array. If the array was empty, the event type was changed to CD and the average time that CD occurred was set as Evt. If a sibling was found, Evt was assigned using the BDCF time array. If the array was empty, CF was changed to CD and the average CD time was set as Evt. If Evt was set, but it was longer than the Evt of its sibling, Evt was made shorter than the sibling's Evt. If the event assigned using the BD list array was BD, Evt was assigned by the BDBD time array. If the array was empty, the average BD time was set as Evt. If Evt was set by the BDBD time array but the Evt was not within -10% to +10% of Evt of its parent cell, Evt was reselected until the Evt fell within this range. If Evt assigned by the BD list array was MD, Evt was assigned by the BDBD time array. If the array was empty, the average BD time was set as Evt. If the event assigned by the BD list array was CD, Evt was assigned the BDCD time array. If the array was empty, the average CD time was set as Evt.

If the current event was MD, information related to its siblings was searched for. If siblings were found and CF was assigned to two siblings, either BD, MD, or CD was assigned by the MD list array, otherwise BD, MD, CF, or CD was assigned. If the event assigned by the MD list array was CF, then, event type of its sibling was again searched. If no sibling was found, Evt was assigned by the MDCF time array. If the array was empty, the event type was changed to CD, and the average time that CD occurred was set as Evt. If only one sibling was found, Evt was assigned by the MDCF time array. If the array was empty, CF was changed to CD and the average CD time was set as Evt. If two siblings were found and CF was assigned to one of the siblings, Evt was assigned by the MDCF time array. If the array was empty, CF was changed to CD and the average CD time was set as Evt. If Evt was longer than the Evt of its siblings, Evt was made shorter than its siblings. If CF was not assigned to any of its siblings, Evt was assigned by the MDCF time array. If the array was empty, CF was changed to CD

and the average CD time was set as Evt. If the event assigned by the MD list array was BD, Evt was assigned by the MDMD time array. If the array was empty, the average BD time was set as Evt. If Evt assigned by the MD list array was MD, Evt was assigned by the MDMD time array. If the array was empty, the average BD time was set as Evt. If the event assigned by the MD list array was CD, Evt was assigned by the MDCD time array. If the array was empty, the average CD time was set as Evt.

Cell-fate simulation algorithm: Readjustment of Evt in cells that underwent CF

If CF occurred in a cell, the Evt of the cell being fused was often affected and the Evt was readjusted (Fig. S7g). If the current event was BD, the next event was assigned by the BDCF lists. If the next event was BD or MD, Evt was assigned by the DivCFDiv time array, and if the next event was CD, Evt was assigned by the BDCFCD array. If the current event was MD, the next event was assigned by the MDCF lists. If the next event was BD or MD, Evt was assigned by the DivCFDiv time array, and if the next event was CD, Evt was assigned by the MDCFCD array.

Cell-fate simulation algorithm: Cell-lineage database creation

The cell-lineage database was created using information held by the CDE (Fig. S7h). If Evt exceeded the simulation time set previously, Evt was adjusted to a time equal to the simulation time. If the event type was BD or MD, information related to the progeny created by BD or MD was entered into the CDE following the generation of corresponding cell numbers for each progeny. If the event type was CF, cells to be fused were searched and relevant information regarding cell-lineage number and cell number was recorded for the cell.

Cell-fate simulation algorithm: Trimming the end of the cell-lineage database

In SS and MCS modes, the end of the cell-lineage data was trimmed to the nearest cell division event (Fig. S7i) before entering the second repeated cycle of assignment.

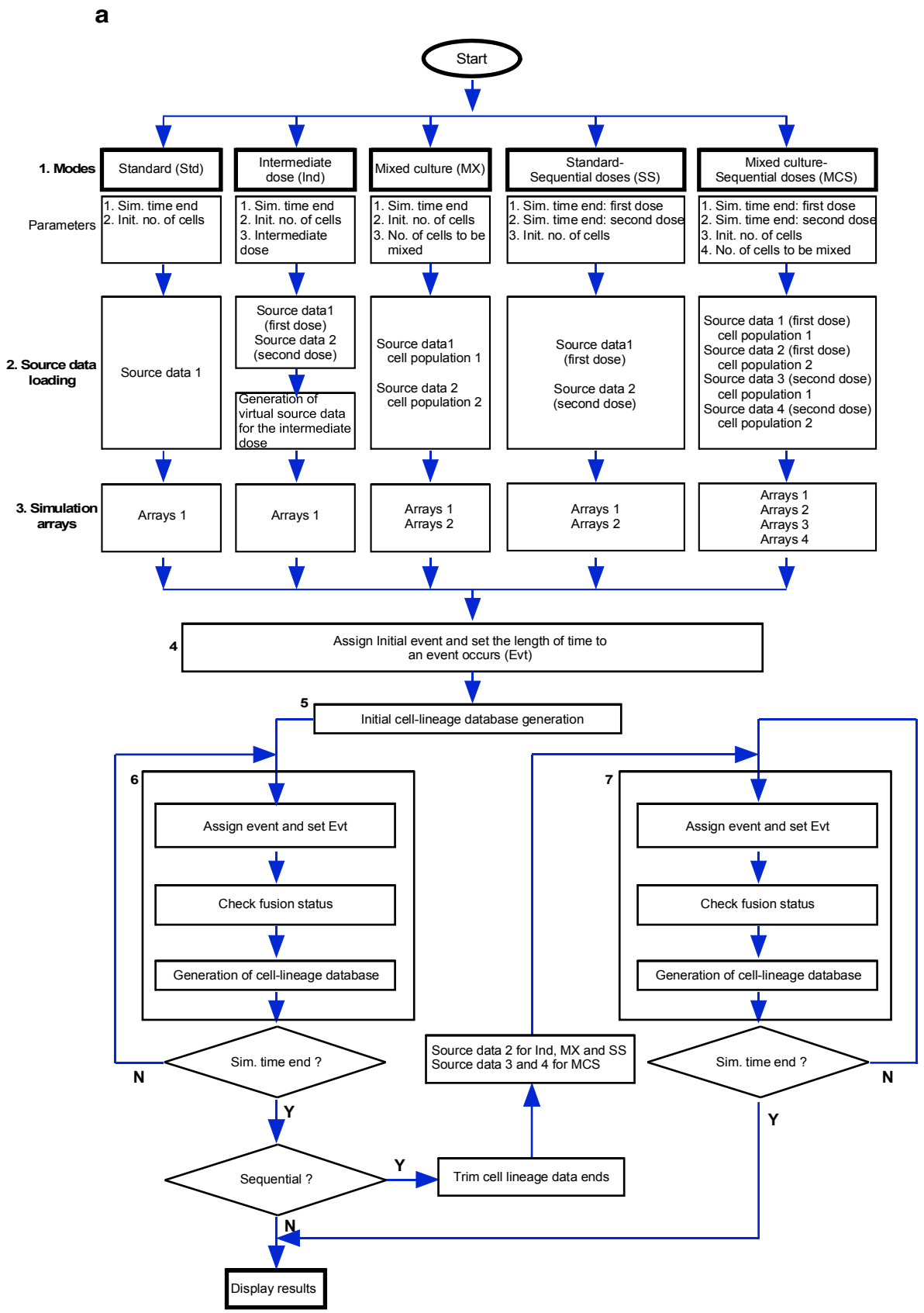
a
Start
1. Modes
Standard (Std)
Intermediate dose (Ind)
Mixed culture (MX)
Standard-Sequential doses (SS)
Mixed culture-Sequential doses (MCS)
Parameters
1. Sim. time end
2. Init. no. of cells
1. Sim. time end
2. Init. no. of cells
3. Intermediate dose
1. Sim. time end
2. Init. no. of cells
3. No. of cells to be mixed
1. Sim. time end: first dose
2. Sim. time end: second dose
3. Init. no. of cells
1. Sim. time end: first dose
2. Sim. time end: second dose
3. Init. no. of cells
4. No. of cells to be mixed
2. Source data loading
Source data 1
Source data1 (first dose)
Source data 2 (second dose)
Generation of virtual source data for the intermediate dose
Source data1 cell population 1
Source data 2 cell population 2
Source data1 (first dose)
Source data 2 (second dose)
Source data 1 (first dose) cell population 1
Source data 2 (first dose) cell population 2
Source data 3 (second dose) cell population 1
Source data 4 (second dose) cell population 2
3. Simulation arrays
Arrays 1
Arrays 1
Arrays 1
Arrays 2
Arrays 1
Arrays 2
Arrays 1
Arrays 2
Arrays 3
Arrays 4
4
Assign Initial event and set the length of time to an event occurs (Evt)
5
Initial cell-lineage database generation
6
Assign event and set Evt
Check fusion status
Generation of cell-lineage database
7
Assign event and set Evt
Check fusion status
Generation of cell-lineage database
Sim. time end ?
N
Y
Source data 2 for Ind, MX and SS
Source data 3 and 4 for MCS
Sim. time end ?
N
Y
Sequential ?
Y
Trim cell lineage data ends
N
Display results

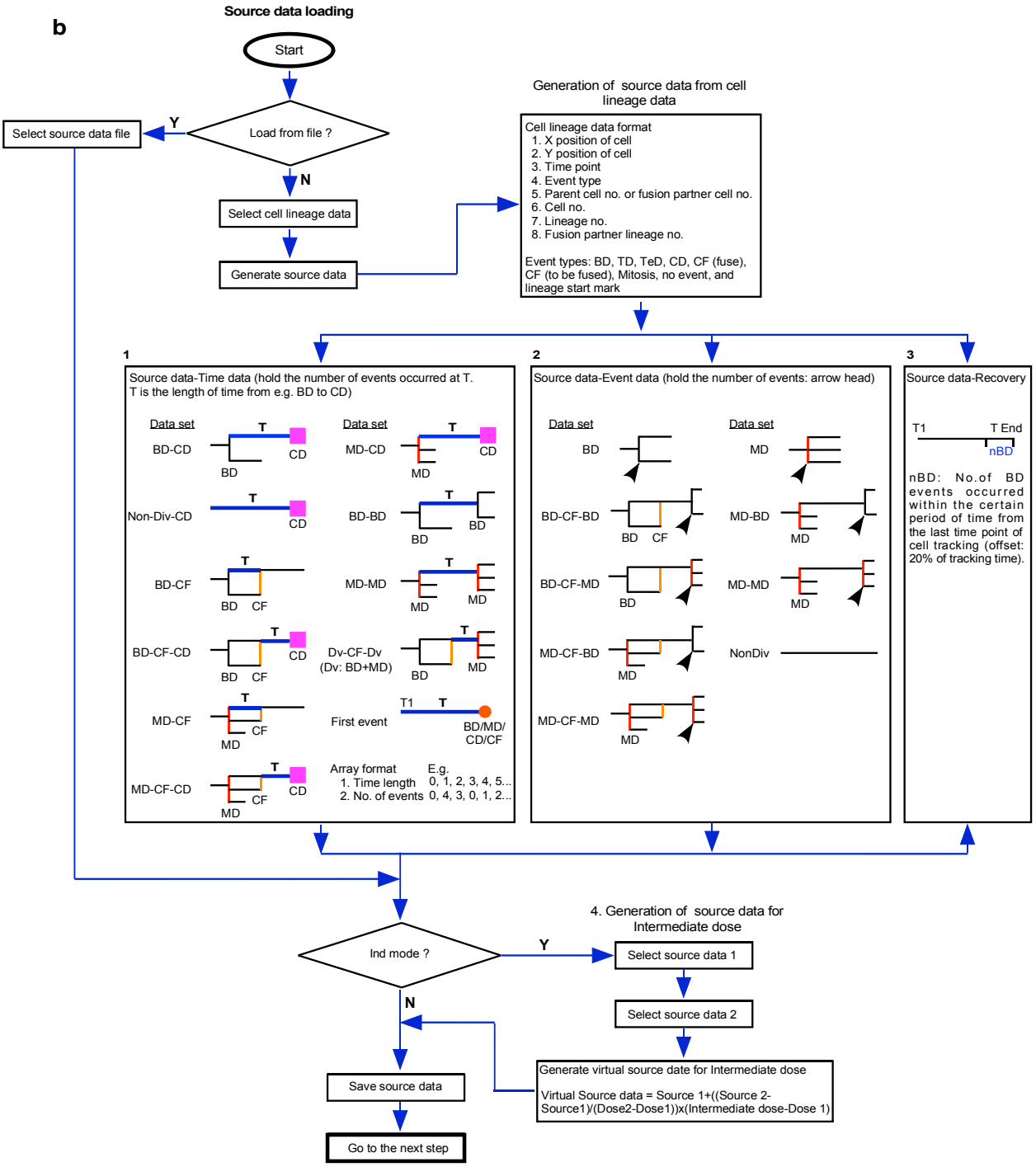
b
Source data loading
Start
Load from file ?
Y
N
Select source data file
Select cell lineage data
Generate source data
Generation of source data from cell lineage data
Cell lineage data format
1. X position of cell
2. Y position of cell
3. Time point
4. Event type
5. Parent cell no. or fusion partner cell no.
6. Cell no.
7. Lineage no.
8. Fusion partner lineage no.
Event types: BD, TD, TeD, CD, CF (fuse), CF (to be fused), Mitosis, no event, and lineage start mark
1
Source data-Time data (hold the number of events occurred at T. T is the length of time from e.g. BD to CD)
Data set
BD-CD
Non-Div-CD
BD-CF
BD-CF-CD
MD-CF
MD-CF-CD
Data set
MD-CD
BD-BD
MD-MD
Dv-CF-Dv
(Dv: BD+MD)
First event
BD/MD/
CD/CF
Array format
1. Time length
2. No. of events
E.g.
0, 1, 2, 3, 4, 5...
0, 4, 3, 0, 1, 2...
2
Source data-Event data (hold the number of events: arrow head)
Data set
BD
BD-CF-BD
BD-CF-MD
MD-CF-BD
MD-CF-MD
Data set
MD
MD-BD
MD-MD
NonDiv
3
Source data-Recovery
T1
T End
nBD
nBD: No.of BD events occurred within the certain period of time from the last time point of cell tracking (offset: 20% of tracking time).
Ind mode ?
Y
N
4. Generation of source data for Intermediate dose
Select source data 1
Select source data 2
Generate virtual source date for Intermediate dose
Virtual Source data = Source 1+((Source 2-Source1)/(Dose2-Dose1))x(Intermediate dose-Dose 1)
Save source data
Go to the next step

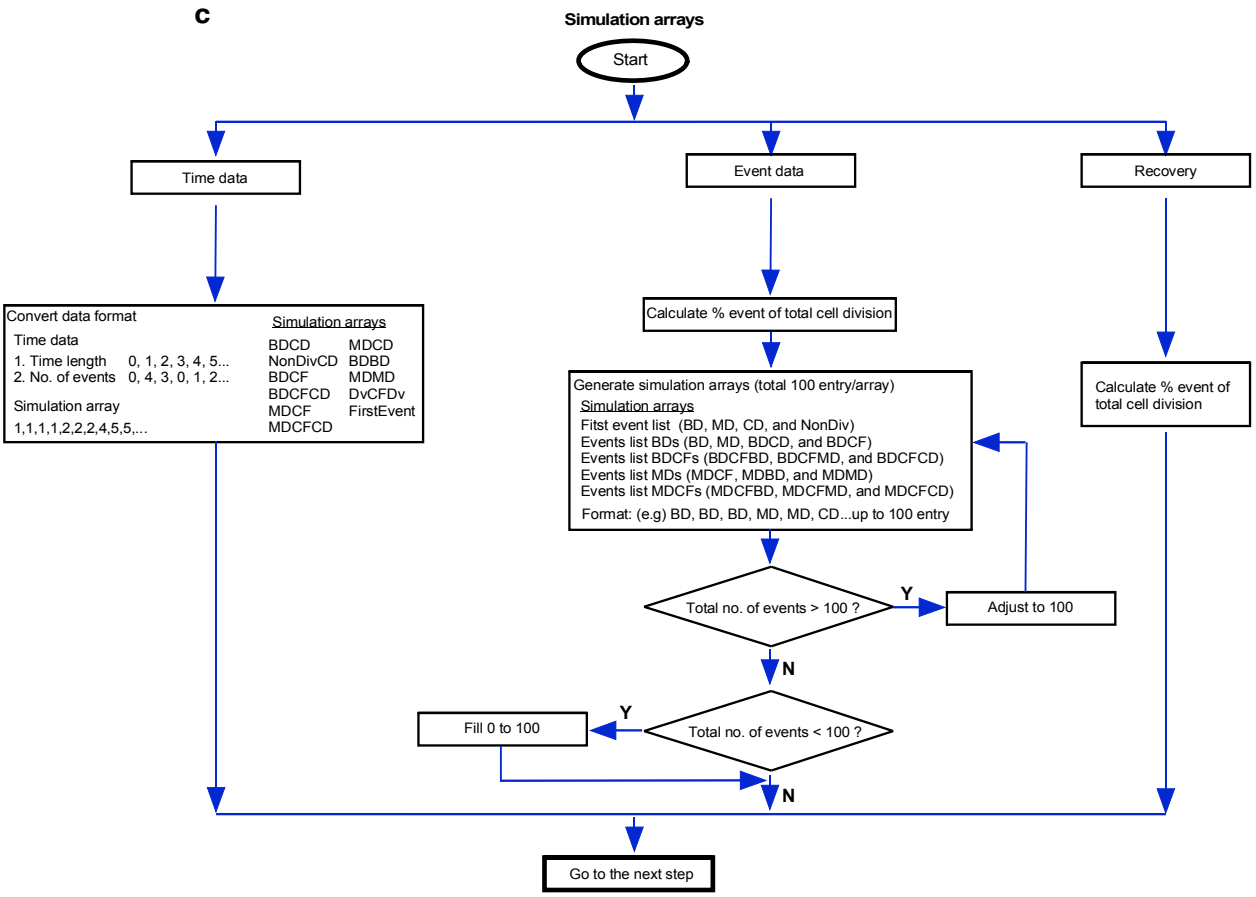
C
Simulation arrays
Start
Time data
Event data
Recovery
Convert data format
Time data
1. Time length 0, 1, 2, 3, 4, 5...
2. No. of events 0, 4, 3, 0, 1, 2...
Simulation array
1,1,1,1,2,2,2,4,5,5,...
Simulation arrays
BDCD MDCD
NonDivCD BDBD
BDCF MDMD
BDCFCD DvCFDv
MDCF FirstEvent
MDCFCD
Calculate % event of total cell division
Generate simulation arrays (total 100 entry/array)
Simulation arrays
Fitst event list (BD, MD, CD, and NonDiv)
Events list BDs (BD, MD, BDCD, and BDCF)
Events list BDCFs (BDCFBD, BDCFMD, and BDCFCD)
Events list MDs (MDCF, MDBD, and MDMD)
Events list MDCFs (MDCFBD, MDCFMD, and MDCFCD)
Format: (e.g) BD, BD, BD, MD, MD, CD...up to 100 entry
Calculate % event of total cell division
Total no. of events > 100 ?
Y
Adjust to 100
N
Total no. of events < 100 ?
Y
Fill 0 to 100
N
Go to the next step

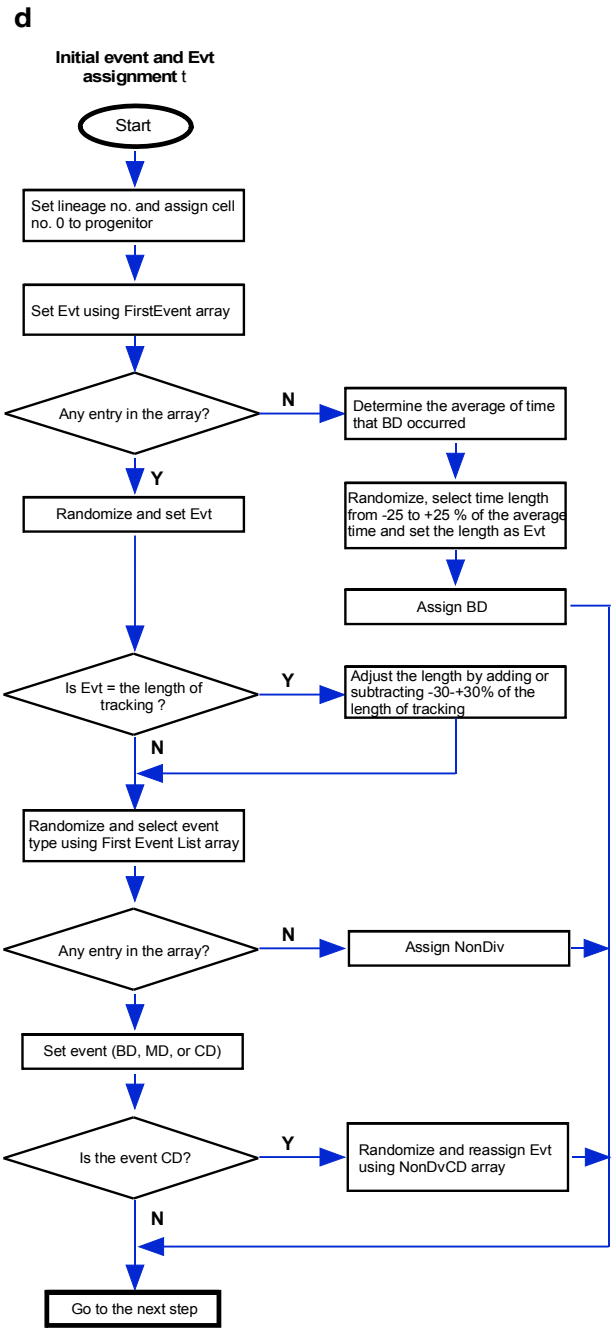
d
Initial event and Evt assignment t
Start
Set lineage no. and assign cell no. 0 to progenitor
Set Evt using FirstEvent array
Any entry in the array?
N
Determine the average of time that BD occurred
Randomize, select time length from -25 to +25 % of the average time and set the length as Evt
Assign BD
Y
Randomize and set Evt
Is Evt = the length of tracking ?
Y
Adjust the length by adding or subtracting -30-+30% of the length of tracking
N
Randomize and select event type using First Event List array
Any entry in the array?
N
Assign NonDiv
Set event (BD, MD, or CD)
Is the event CD?
Y
Randomize and reassign Evt using NonDvCD array
N
Go to the next step

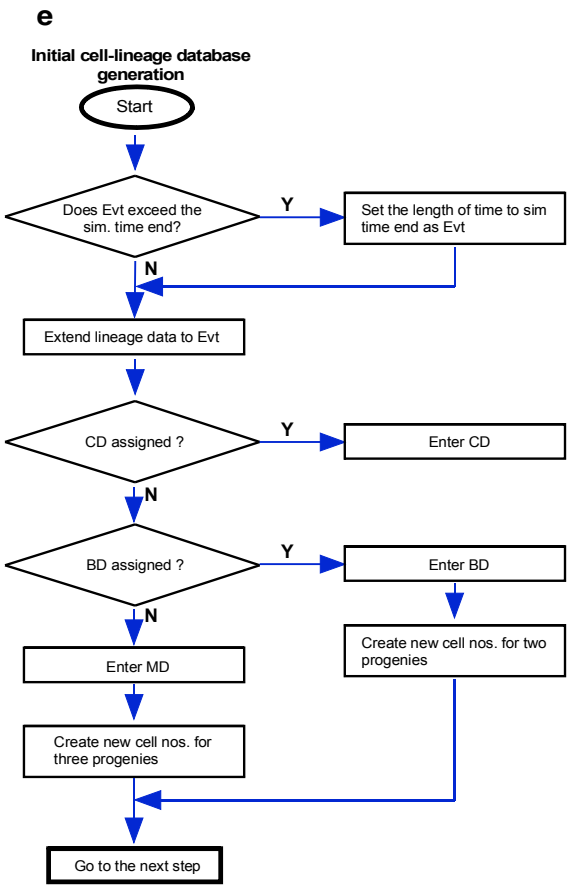
e
Initial cell-lineage database generation
Start
Does Evt exceed the sim. time end?
Y
Set the length of time to sim time end as Evt
N
Extend lineage data to Evt
CD assigned ?
Y
Enter CD
N
BD assigned ?
Y
Enter BD
Create new cell nos. for two progenies
N
Enter MD
Create new cell nos. for three progenies
Go to the next step

f

Assignment of events and Evt

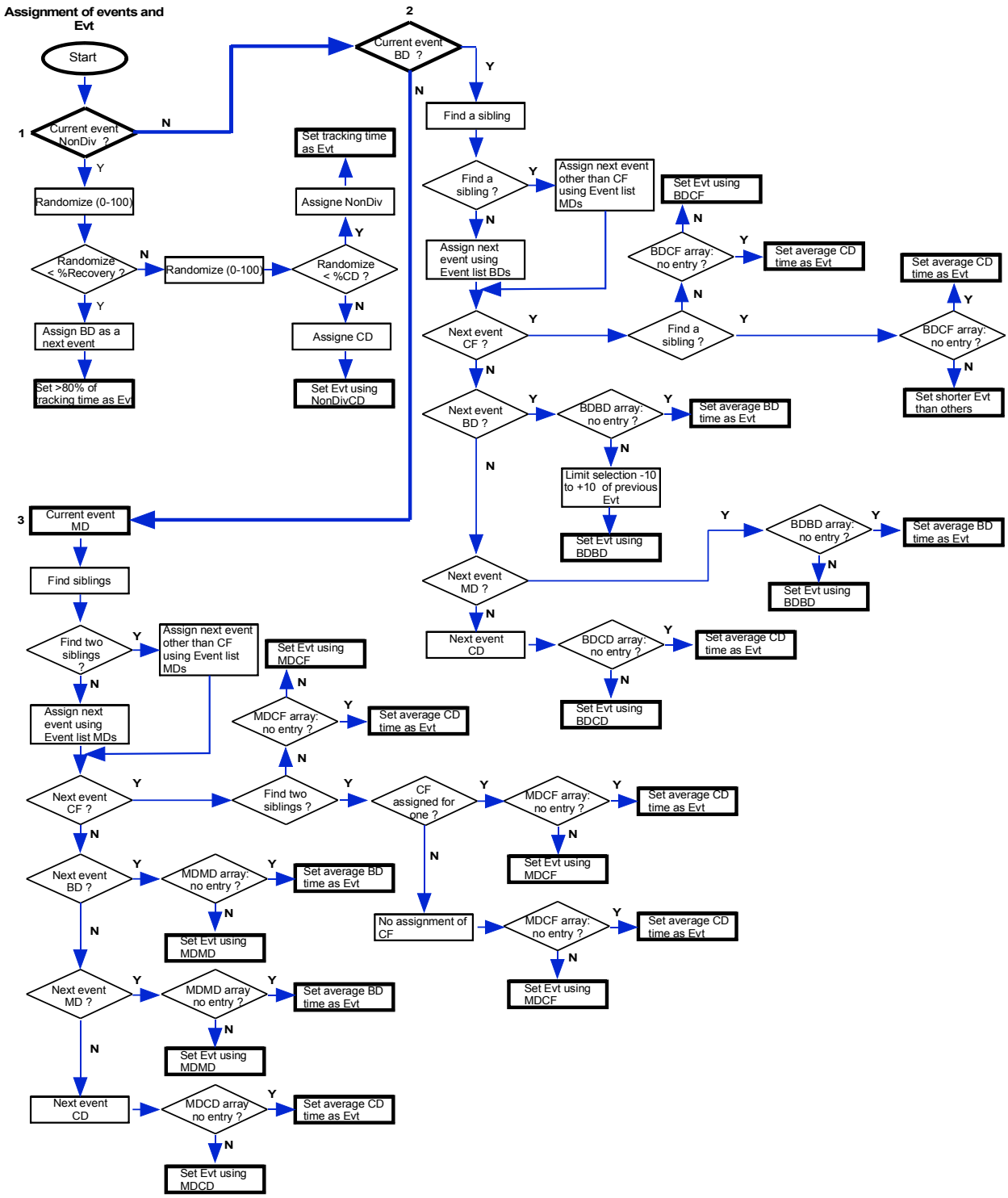

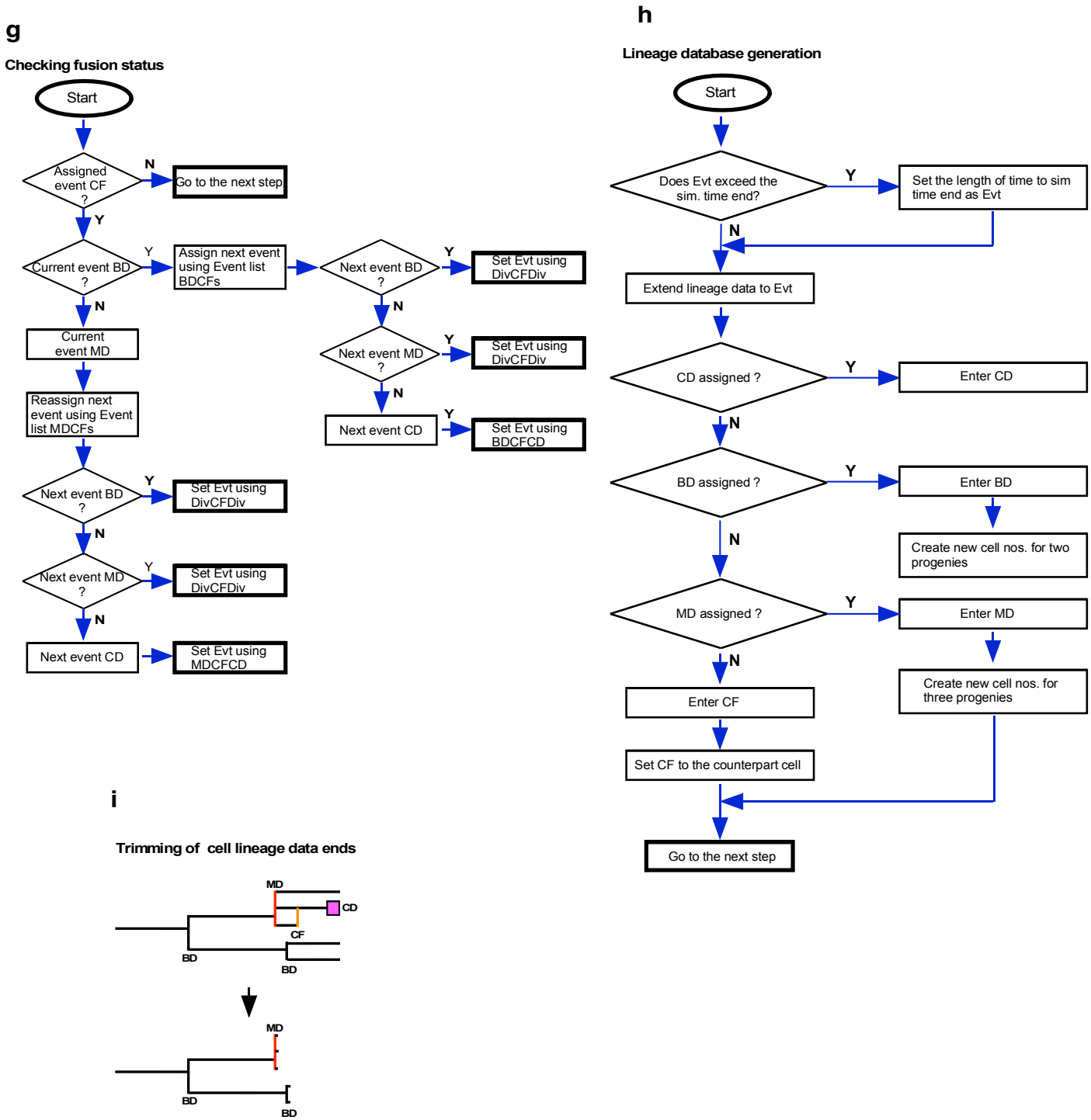

Supplementary Figure 7. Cell-fate simulation algorithm. Outlines of the cell fate simulation algorithm are shown. (**a**) Overall summary of the algorithm, (**b**) creation of Source data and its types, (**c**) simulation arrays and its format, (**d**) initial event assignment, (**e**) initial cell-lineage database generation, (**f**) main event assignment algorithm, (**g**) re-assignment of events in cases with CF, (**h**) cell-lineage database generation, and (**i**) trimming of cell-lineage data ends to switch from the first to second Source data.

Statistical analysis.

Statistical analyses were performed by Prism 8.

ACKNOWLEDGEMENTS

We thank Amélie Fradet-Turcotte for critical reading of the manuscript. We like to acknowledge the Bioimaging Platform of Research Centre for Infectious Diseases for the technical support of microscopes. This work was supported by the Canadian Foundation for Innovation and Canadian Institutes for Health Research.

AUTHOR CONTRIBUTIONS

M.S.S. and S.S. designed this work, performed the experiments, and wrote the paper. M.S.S developed the cell-fate simulation algorithm. A.R. performed the experiments and single-cell tracking analysis and edited the paper.

DECLARATION OF INTERESTS

The authors declare no competing interests.

DATA AND CODE AVAILABILITY STATEMENT

The datasets and code supporting the current study have not been deposited in a public repository because standard formats for the dataset and processing procedure for the code have not yet been standardized, but are available from the corresponding author on request.

REFERENCES

1. Basanta, D. & Anderson, A.R.A. Homeostasis Back and Forth: An Ecoevolutionary Perspective of Cancer. *Cold Spring Harb Perspect Med* **7** (2017).
2. Kandoth, C. et al. Mutational landscape and significance across 12 major cancer types. *Nature* **502**, 333-339 (2013).
3. Hollstein, M., Sidransky, D., Vogelstein, B. & Harris, C.C. p53 mutations in human cancers. *Science* **253**, 49-53 (1991).
4. Petitjean, A. et al. Impact of mutant p53 functional properties on TP53 mutation patterns and tumor phenotype: lessons from recent developments in the IARC TP53 database. *Hum Mutat* **28**, 622-629 (2007).
5. Boutelle, A.M. & Attardi, L.D. p53 and Tumor Suppression: It Takes a Network. *Trends Cell Biol* **31**, 298-310 (2021).
6. Levine, A.J. The many faces of p53: something for everyone. *J Mol Cell Biol* **11**, 524-530 (2019).
7. Kastenhuber, E.R. & Lowe, S.W. Putting p53 in Context. *Cell* **170**, 1062-1078 (2017).
8. Lavin, M.F. & Gueven, N. The complexity of p53 stabilization and activation. *Cell Death Differ* **13**, 941-950 (2006).
9. Vogelstein, B., Lane, D. & Levine, A.J. Surfing the p53 network. *Nature* **408**, 307-310 (2000).
10. Hafner, A., Bulyk, M.L., Jambhekar, A. & Lahav, G. The multiple mechanisms that regulate p53 activity and cell fate. *Nat Rev Mol Cell Biol* **20**, 199-210 (2019).
11. Livingstone, L.R. et al. Altered cell cycle arrest and gene amplification potential accompany loss of wild-type p53. *Cell* **70**, 923-935 (1992).
12. Kastan, M.B. et al. Levels of p53 protein increase with maturation in human hematopoietic cells. *Cancer Res* **51**, 4279-4286 (1991).

13. Clarke, A.R. et al. Thymocyte apoptosis induced by p53-dependent and independent pathways. *Nature* **362**, 849-852 (1993).

14. Lowe, S.W., Schmitt, E.M., Smith, S.W., Osborne, B.A. & Jacks, T. p53 is required for radiation-induced apoptosis in mouse thymocytes. *Nature* **362**, 847-849 (1993).

15. Campisi, J. Senescent cells, tumor suppression, and organismal aging: good citizens, bad neighbors. *Cell* **120**, 513-522 (2005).

16. Rufini, A., Tucci, P., Celardo, I. & Melino, G. Senescence and aging: the critical roles of p53. *Oncogene* **32**, 5129-5143 (2013).

17. Haupt, Y., Maya, R., Kazaz, A. & Oren, M. Mdm2 promotes the rapid degradation of p53. *Nature* **387**, 296-299 (1997).

18. Honda, R., Tanaka, H. & Yasuda, H. Oncoprotein MDM2 is a ubiquitin ligase E3 for tumor suppressor p53. *FEBS Lett* **420**, 25-27 (1997).

19. Kubbutat, M.H., Jones, S.N. & Vousden, K.H. Regulation of p53 stability by Mdm2. *Nature* **387**, 299-303 (1997).

20. Guo, S. et al. Nonstochastic reprogramming from a privileged somatic cell state. *Cell* **156**, 649-662 (2014).

21. Vousden, K.H. & Lane, D.P. p53 in health and disease. *Nat Rev Mol Cell Biol* **8**, 275-283 (2007).

22. Kruiswijk, F., Labuschagne, C.F. & Vousden, K.H. p53 in survival, death and metabolic health: a lifeguard with a licence to kill. *Nat Rev Mol Cell Biol* **16**, 393-405 (2015).

23. Lassus, P., Ferlin, M., Piette, J. & Hibner, U. Anti-apoptotic activity of low levels of wild-type p53. *EMBO J* **15**, 4566-4573 (1996).

24. Chow, K.K. et al. Imaging cell lineage with a synthetic digital recording system. *Science* **372** (2021).

25. Chapal-Ilani, N. et al. Comparing algorithms that reconstruct cell lineage trees utilizing information on microsatellite mutations. *PLoS Comput Biol* **9**, e1003297 (2013).

26. Zafar, H., Lin, C. & Bar-Joseph, Z. Single-cell lineage tracing by integrating CRISPR-Cas9 mutations with transcriptomic data. *Nat Commun* **11**, 3055 (2020).

27. Boveri, T. Concerning the origin of malignant tumours by Theodor Boveri. Translated and annotated by Henry Harris. *J Cell Sci* **121 Suppl 1**, 1-84 (2008).

28. Keryer, G., Ris, H. & Borisy, G.G. Centriole distribution during tripolar mitosis in Chinese hamster ovary cells. *J Cell Biol* **98**, 2222-2229 (1984).

29. Holland, A.J. & Cleveland, D.W. Boveri revisited: chromosomal instability, aneuploidy and tumorigenesis. *Nat Rev Mol Cell Biol* **10**, 478-487 (2009).

30. Gisselsson, D. et al. When the genome plays dice: circumvention of the spindle assembly checkpoint and near-random chromosome segregation in multipolar cancer cell mitoses. *PLoS One* **3**, e1871 (2008).

31. Saunders, W. Centrosomal amplification and spindle multipolarity in cancer cells. *Semin Cancer Biol* **15**, 25-32 (2005).

32. Emdad, L., Sarkar, D., Su, Z.Z. & Fisher, P.B. Emerging roles of centrosomal amplification and genomic instability in cancer. *Front Biosci* **10**, 728-742 (2005).

33. Williams, A.B. & Schumacher, B. p53 in the DNA-Damage-Repair Process. *Cold Spring Harb Perspect Med* **6** (2016).

34. Valente, L.J. et al. p53 deficiency triggers dysregulation of diverse cellular processes in physiological oxygen. *J Cell Biol* **219** (2020).

35. Riethmuller, G. & Klein, C.A. Early cancer cell dissemination and late metastatic relapse: clinical reflections and biological approaches to the dormancy problem in patients. *Semin Cancer Biol* **11**, 307-311 (2001).

36. Husemann, Y. et al. Systemic spread is an early step in breast cancer. *Cancer Cell* **13**, 58-68 (2008).

37. Risson, E., Nobre, A.R., Maguer-Satta, V. & Aguirre-Ghiso, J.A. The current paradigm and challenges ahead for the dormancy of disseminated tumor cells. *Nat Cancer* **1**, 672-680 (2020).

38. Sosa, M.S. et al. NR2F1 controls tumour cell dormancy via SOX9- and RARbeta-driven quiescence programmes. *Nat Commun* **6**, 6170 (2015).

39. Eischen, C.M. Genome Stability Requires p53. *Cold Spring Harb Perspect Med* **6** (2016).

40. Dutertre, S., Hamard-Peron, E., Cremet, J.Y., Thomas, Y. & Prigent, C. The absence of p53 aggravates polyploidy and centrosome number abnormality induced by Aurora-C overexpression. *Cell Cycle* **4**, 1783-1787 (2005).

41. Deangelis, P. et al. P53 expression is associated with a high-degree of tumor DNA aneuploidy and incidence of p53 gene mutation, and is localized to the aneuploid component in colorectal carcinomas. *Int J Oncol* **3**, 305-312 (1993).

42. Ramel, S. et al. Inactivation of p53 and the development of tetraploidy in the elastase-SV40 T antigen transgenic mouse pancreas. *Pancreas* **11**, 213-222 (1995).

43. Galipeau, P.C. et al. 17p (p53) allelic losses, 4N (G2/tetraploid) populations, and progression to aneuploidy in Barrett's esophagus. *Proc Natl Acad Sci U S A* **93**, 7081-7084 (1996).

44. Harvey, M. et al. In vitro growth characteristics of embryo fibroblasts isolated from p53-deficient mice. *Oncogene* **8**, 2457-2467 (1993).

45. Fujiwara, T. et al. Cytokinesis failure generating tetraploids promotes tumorigenesis in p53-null cells. *Nature* **437**, 1043-1047 (2005).

46. Thompson, S.L. & Compton, D.A. Examining the link between chromosomal instability and aneuploidy in human cells. *J Cell Biol* **180**, 665-672 (2008).

47. Vitale, I. et al. Multipolar mitosis of tetraploid cells: inhibition by p53 and dependency on Mos. *EMBO J* **29**, 1272-1284 (2010).

48. Aylon, Y. & Oren, M. p53: guardian of ploidy. *Mol Oncol* **5**, 315-323 (2011).

49. Ganem, N.J., Storchova, Z. & Pellman, D. Tetraploidy, aneuploidy and cancer. *Curr Opin Genet Dev* **17**, 157-162 (2007).

50. Storchova, Z. & Kuffer, C. The consequences of tetraploidy and aneuploidy. *J Cell Sci* **121**, 3859-3866 (2008).

51. Shi, Q. & King, R.W. Chromosome nondisjunction yields tetraploid rather than aneuploid cells in human cell lines. *Nature* **437**, 1038-1042 (2005).

52. Wu, S., Bafna, V. & Mischel, P.S. Extrachromosomal DNA (ecDNA) in cancer pathogenesis. *Curr Opin Genet Dev* **66**, 78-82 (2021).

53. Sato, S., Rancourt, A., Sato, Y. & Satoh, M.S. Single-cell lineage tracking analysis reveals that an established cell line comprises putative cancer stem cells and their heterogeneous progeny. *Sci Rep* **6**, 23328 (2016).

54. Sato, S., Rancourt, A. & Satoh, M.S. Identification of SNA-I-positive cells as stem-like cells in an established cell line using computerized single-cell lineage tracking. *BioRxiv* **508705; doi: https://doi.org/10.1101/508705** (2018).

FIGURE LEGENDS

Figure 1. System for investigating the functional implications of maintaining low cell levels of p53. A549 cells were cultured on multi-well chamber slides and the areas of interest were scanned. Cells were treated with scrambled siRNA or p53 siRNA in the presence or absence of various doses of MNNG, and the cell responses were monitored to generate live cell imaging videos. The videos were used for imaging and single-cell tracking, starting immediately after MNNG treatment. Progenitors were selected from the image designated as tracking time 0 min (T0), and the progenitors and their progeny were tracked empirically. Each cell-linage dataset comprised tracking results for one progenitor and their progeny, and any events that occurred in the cells. A cell-lineage map was generated from the dataset, and the cell-lineage database contains multiple cell-lineage datasets. Quantitative bioinformatics analysis was performed using the database, which was also used to develop a cell-fate simulation algorithm.

Figure 2. Cell-population expansion rates determined by cell counting and single-cell tracking analysis. Control (**a**) and p53si (**b**) cells were exposed to 1, 3, and 7 μM MNNG to give Control and MNNG1, MNNG3, and MNNG7 cells, and p53si and p53si-MNNG1, p53si-MNNG3, and p53si-MNNG7 cells, respectively. (**a-f**) Images were divided into a 5 × 5 squares and cell population expansion curves were determined by counting the number of cells in a square (~ 512 × 512 pixels) at 1,000 min intervals (see Fig. S5). Fifteen squares were selected from three independently generated videos. Expansion curves were compared as follows: Control vs. p53si (**c**), MNNG1 vs. p53si-MNNG1 (**d**), MNNG3 vs. p53si-MNNG3 (**e**), and MNNG7 vs. p53si-MNNG7 (**f**) cells. Student's *t*-test (**c-f**) and ordinary one-way ANOVA (Tukey's) (**a** and **b**) were performed (n=15), and standard errors are shown. (**g** and **h**) Cell population expansion curves of Control (**g**) and p53si (**h**) cells were determined using a cell-lineage database. Single-cell tracking was performed for 4,000 min with videos acquired at 10 min intervals (n=399). The number of cells every 10 min was calculated and plotted. Growth curves were

compared as follows: Control vs. p53si (**i**), MNNG1 vs. p53si-MNNG1 (**j**), MNNG3 vs. p53si-MNNG3 (**k**), and MNNG7 vs. p53si-MNNG7 (**l**) cells. (**i-l**) The data were analyzed by Student's *t*-tests in the following approach. The difference in cell numbers between n and n+10 min was calculated (e.g. if the numbers of cells at 10 and 20 min were 100 and 103, the difference was 3). (**a-f** and **i-l**) NS: non-significant, $^{*}P < 0.05$, $^{**}P < 0.01$, $^{***}P < 0.001$, $^{****}P < 0.0001$.

Figure 3. Number of progeny produced from a progenitor. (**a**) The number of progeny produced from a progenitor was calculated, as shown in (**c**). If a progenitor produced two progeny at a tracking time of 4,000 min, this lineage was categorized as No. of progenies/lineage = 1–3, with No. of cells = 2. Similarly, if four progeny were produced, the lineage was categorized as No. of progenies/lineage = 4–6, and No. of cells = 4. Values shown in (**a**) are number of lineages. (**b**) Differences relative to the No. of Control cells were also calculated. Blue and red bars represent groups in the cell lineage that were increased (blue) or decreased (red) relative to the Control cells after silencing and/or MNNG treatment.

Figure 4. Analysis of MD, CD, and CF using counting and single-cell tracking analysis. Control and p53si cells were exposed to 1, 3, and 7 μM MNNG to produce Control and MNNG1, MNNG3, and MNNG7 cells, and p53si and p53si-MNNG1, p53si-MNNG3, and p53si-MNNG7 cells, respectively. The numbers of MD (**a**) and CD (**b**) events that occurred during the tracking time (4,000 min) were determined by counting. Three independently generated videos were used and counting was thus performed (see Fig. S6a) in 12 squares. The numbers of MD (**c**), CD (**d**), and CF (**e**) events that occurred during the tracking time (4,000 min) were determined using a cell-lineage database. The numbers of MD, CD, and CF events in each cell lineage were determined (n=335). (**a-e**) Statistical analysis was performed by ordinary one-way ANOVA (Tukey's). NS: non-significant, $^{*}P < 0.05$, $^{**}P < 0.01$, $^{***}P < 0.001$, $^{****}P < 0.0001$. Standard errors are shown.

Figure 5. *In silico* generation of cell-lineage database. (**a**) *In silico* generation of cell-lineage database for the evaluation of the impact of CD on the population expansion. If the growth of a cell was terminated by CD, e.g. C3, the corresponding cell-lineage data were replaced with cell-lineage data for its sibling (C2) *in silico*, creating cells C6 and C7. (**b**) A cell population expansion curve was generated using the *in silico*-created cell-lineage database for Control and p53si cells (Control-Sil(-CD) and p53si-Sil(-CD), respectively). At a tracking time of 4,000 min, CD resulted in a 7.4% reduction in the population size of p53si cells. The frequency of CD (red lines) occurring during tracking is also shown. Statistical analysis was performed by ordinary one-way ANOVA (Tukey's). $^{*}P < 0.05$.

Figure 6. Events leading to the induction of MD. (**a**) Cellular events that occurred prior to MD were analyzed by tracing cell-lineages backwards. (**b**) Cells that underwent CF were determined by tracing cell-lineages backwards. (**c**) Progeny produced by MD were tracked and the number of progeny that underwent BD was determined. (**d**) The number of MD events was plotted against the number of BD events. Numbers in (**d**) indicate the doses of MNNG.

Figure 7. Simulations of effects of p53 silencing and MNNG exposure on cell population expansion. Simulations were performed using Source data generated from cell-lineage data, Control, and MNNG1, MNNG3, and MNNG7, and p53si, and p53si-MNNG1, p53si-MNNG3, and p53si-MNNG7 with a total of 5,000 virtual progenitors for a simulation time of 15,000 min. (**a** and **b**) Virtual cell population expansion curves of Control-Sim cells and cells exposed to various doses of MNNG (**a**: 0–4,000 min, and **b**: whole scale, 0–15,000 min). (**c**, **d**, **e**, and **f**) Data obtained from the simulation were compared with growth curves determined by empirical single-cell tracking analysis; (**c**) Control, (**d**) MNNG1, (**e**) MNNG3, and (**f**) MNNG7). Difference (%) was determined by obtaining the sum of the number of Empirical cells/the number of Simulated cells determined at each simulation time point

divided by 1,500 simulation time × 100. For example, a difference of 2.7% implied that the simulation generated 2.7% more cells compared with the Empirical data. (**g** and **h**) Virtual cell growth curves of p53si-Sim cells and cells exposed to various doses of MNNG (**g**: 0–4,000 min, and **h**: whole scale, 0–15,000 min). (**i**, **j**, **k**, and **l**) These simulation data were compared with the cell population expansion curves determined by empirical single-cell tracking analysis; (**i**) p53si, (**j**) p53si-MNNG1, (**k**) p53si-MNNG3, and (**l**) p53si-MNNG7). Results of simulation obtained using Source data-p53si-Sil(-CD) were also included in **g** and **h**.

Figure 8. Virtual dose-response analysis and damage response. Virtual Source data corresponding to each 0.5 μM dose of MNNG was generated in Ind mode using Source data-Control, MNNG1, MNNG3, and MNNG7, p53si, p53si-MNNG1, p53si-MNNG3, and p53si-MNNG7. (**a**) Virtual cell growth curves generated by the simulation using Source data-Control to 1.5 (blue), 2–3 (orange), 3.5–6.5 (green), and 7 (red) are shown. (**b**) Virtual dose-response curves generated by the simulation using Source data-p53si to 1.5 (purple), 2–3 (pink), 3.5–6.5 (dark green), and 7 (marron) are shown. The numbers of cells at simulation times of 4,000 and 15,000 min were plotted on **c** and **d**, respectively. Standard deviations are shown. Results of single-cell tracking analysis are also indicated in **c**. (**e**) Time necessary to reach a cell population to be doubled (100 to 200 cells) was determined by Std mode using Source data-Control, MNNG7, p53si, and p53si-MNNG7. The difference in time between MNNG7-Sim (9,651 min) and Control-Sim (2,501 min) was 7,150 min. Similarly, the difference in doubling time between p53si-MNNG7-Sim and p53si-Sim was 4,510 min. Assuming that the difference in doubling time between MNNG7-Sim and Control-Sim represents the direct effect of MNNG and damage response, while that between p53si-MNNG7-Sim and p53si-Sim only represents the direct effect of MNNG, 63.1% and 36.9% of growth suppression in MNNG7-Sim were likely to be due to the direct effect of MNNG and the damage responses induced by the stabilization of p53, respectively.

Figure 9. Simulation of growth of the progeny of MD. The simulation was performed using Source data-Control (**a-c**) and p53si (**d-f**) in Std mode. (**g**) The progeny of MD and those that underwent BD were indicated in burgundy and green, respectively. All other progeny were shown as gray. The simulation was carried out for 2,500 progeny, which generated 6.6×10^6 cells during the 20,000 min of simulation. (**a** and **b**) Whole-scale and magnified images generated by the simulation using the Source data-Control are shown in **a** and **b**, respectively. An animation was created to visualize the growth of the cells (Movie S3) and an image at simulation time 20,000 min is shown (**c**). (**d** and **e**) Whole-scale and magnified images generated by the simulation using Source data-p53si are shown in **d** and **e**, respectively. An animation was created to visualize the growth of the cells (Movie S4) and an image at simulation time 20,000 min is shown (**f**).

Figure 10. Limiting expansion of p53-silenced cells in a p53-expressing cell population. We simulated the expansion of the p53-silenced cell population (4% at the initial time point) in a p53-expressing cell population (96% at the initial time point) using MX mode with source data-Control and p53si for a simulation time of 20,000 min with 500 progenitors and repeating 10 simulations (total 5000 progenitors). (**a**) Simulation of 480 p53-expressing progenitors was carried out using Source data-Control and 20 p53-silenced progenitors with Source data-p53si. The initial percentage of p53-silenced cells was 4%, which was reduced to 2.4% at 20,000 min. (**b**) The sums of MD, CD, and CF events are shown. (**c** and **d**) Still images of the animation (Movie S5) at simulation times 0 and 20,000 min are also shown in **c** and **d**, respectively. (**e** and **f**) Simulation was performed using Source data-p53si-Sil(-CD) (**e**), and a still image of the animation at 20,000 min is shown (**f**). In the animation, p53-silenced cells are indicated in blue.

Figure 11. Expansion of p53-silenced cells in a p53-expressing cell population subjected to virtual MNNG exposure. We simulated the response of p53-silenced cells in a p53-expressing cell population

to MNNG exposure using MCS mode. (**a**) The simulation was performed with 96% p53-expressing and 4% p53-silenced cells, using Source data-Control and p53si for 9900 min. The Source data was then switched to e.g. MNNG7 and p53si-MNNG7 for virtual MNNG treatment, and the simulation was continued up to 20,000 min. In the animation (Movie S6), the brightness of the image was changed to indicate the virtual MNNG treatment. (**b**, **d**, **f**, **h**, and **j**) In the simulation, virtual source data corresponding to (**b**) 1.5, (**d**) 3, (**f**) 5, (**h**) 6, and (**j**) 7 μM MNNG were created to perform a MNNG treatment. The numbers in the images indicate the percent of p53-silenced cells at simulation times 0 and 20,000 min. (**c**, **e**, **g**, **i**, and **k)** Still images from animations for (**c**) 1.5, (**e**) 3, (**g**) 5, (**i**) 6, and (**k**) 7 μM MNNG at 20,000 min are shown. (**l**) The percentages of p53-silenced cells in the population were plotted. Statistical analysis (n=10) was performed using data at simulation time 20,000 min by ordinary one-way ANOVA. NS: nonsignificant, $^{*}P < 0.05$, $^{****}P < 0.0001$. (**m**) Based on the simulation data for 7 μM MNNG, percentage of p53-silenced cells following repeated 7 μM MNNG exposure was calculated. Arrows indicate the time that the virtual exposure was performed.

Figure 12. Role of the low level of p53 in maintaining the integrity of cells and damage response. (**a**) Characteristics of p53-expressing and p53-silenced cells. (**b**) Different fates of p53-silenced cells under unstressed and stressed conditions.

SUPPLEMENTARY FIGURES

Supplementary Figure 1. Events occurring in the cells. Cellular events that occurred in A459 cells were categorized as follows: bipolar cell division (BD), tripolar cell division, tetrapolar cell division, cell death (CD), and cell fusion (CF). In the current study, tripolar and tetrapolar cell divisions were defined as multipolar cell division (MD). Green arrowheads indicate cells that underwent an event. Red arrowheads indicate daughter cells, a dead cell, and a fused cell.

Supplementary Figure 2. Cell-density analysis. Cell density maps were created using a heat map scale. (**a**) Still images taken from Movie S1. Cell density map created by assigning value 1 to a pixel within the 20-pixel diameter area from the position of a cell (blue); if an area overlapped with other areas, the pixel was assigned the sum of the number of overlapped areas (light green) (**b**). These values were used to generate heat maps. Cell density and average cell size every 10 min were plotted (**c**).

Supplementary Figure 3. Determination of minimum number of cell-lineage datasets required to build a cell-lineage database. A cell-lineage database containing 50–240 cell-lineage datasets was used to determine cell population expansion curves. (**a-e**) Cell population expansion curves determined based on cell-lineage databases containing 50 (**a**), 80 (**b**), 120 (**c**), 140 (**d**), and 240 (**e**) datasets. The number of cells every 10 min was calculated using the database and plotted. The analysis was repeated three times (green, orange, and red lines) to show variations at a tracking time of 4,000 min (black bars). (**f**) Variations of 4,000 min were plotted.

Supplementary Figure 4. Accumulation of particles following siRNA transfection and analysis of p53 expression following transfection and/or MNNG exposure. (**a**) Particles formed following siRNA transfection are shown. DIC and objects with brightness 150–254 and size 5–30 pixels were

extracted from the DIC image (Particles). (**b**) The numbers of particles at five different locations in the image were plotted. Blue lines represent the average number of particles at each time point and the red line shows the overall average. MNNG treatment was performed after approximately 1,740 min of siRNA transfection, and continued for 30 min. The number of particles peaked at 3,750 min after transfection. Single-cell tracking was started immediately after MNNG treatment and continued for 4,000 min. (**c**) Western blotting with anti-p53 antibody was performed 48 h after siRNA treatment. Amounts of p53 relative to Control are shown.

Supplementary Figure 5. Determination of cell-population expansion rate using video images. A video image (typically 2560 pixels x 2560 pixels) was divided into 5 x 5 squares and the numbers of cells in selected squares were counted. Counting was performed every 1,000 min in video images from 0–4,000 min.

Supplementary Figure 6. Counting MD and CD using live-cell imaging videos. (**a**) Each time point of the video image was divided into four squares, and CD and MD events in each square were marked to determine the overall numbers of events that occurred during imaging. Three independently generated videos were used, and 12 squares were thus counted. The positions of MD and CD events were also stacked to generate MD and CD density maps. MD (**b**) and CD (**c**) density maps were created using a similar approach to cell density determination (see Fig. S2b). Density was shown using a heat map scale. Black squares correspond to the area used for single-cell tracking.

Supplementary Figure 7. Cell-fate simulation algorithm. Outlines of the cell fate simulation algorithm are shown. (**a**) Overall summary of the algorithm, (**b**) creation of Source data and its types, (**c**) simulation arrays and its format, (**d**) initial event assignment, (**e**) initial cell-lineage database generation, (**f**) main event assignment algorithm, (**g**) re-assignment of events in cases with CF, (**h**) cell-

lineage database generation, and (**i**) trimming of cell-lineage data ends to switch from the first to second Source data.

Supplementary Figure 8. Cell-lineage maps generated by single-cell tracking and a cell-fate simulation algorithm. (**a**) Cell-lineage maps generated by cell-lineage database Control cells. The single-cell tracking analysis created 335 cell-lineage datasets, and 16 cell-lineage maps are shown. (**b**) Cell-lineage maps generated by simulation using source data-p53si. The simulation created 2,500–5,000 virtual cell-lineage datasets, and 16 cell-lineage maps generated from the virtually created cell-lineage datasets are shown. Light blue circle, mitosis; pink square, CD; orange circle and orange vertical line, CF; black vertical line, BD; red vertical line, MD.

Supplementary Figure 9. Determination of number of progenitors required to perform a reproducible simulation. The simulation was performed with 300–2,000 progenitors using either the Source data-Control (**a**) or Source data-MNNG7 (**b**). Each simulation was repeated five times and virtual cell-lineage databases for Control-Sim and MNNG7-Sim cells were created to determine the population expansion curves of the virtual cells. The percentage of variation relative to the average at simulation time 15,000 min is also shown.

Supplementary Figure 10. Cell-doubling time distribution. Cell-doubling time distribution was determined using the cell-linage database (Empirical) and simulation (Simulation) data. (**a**, **b**, **c**, and **d**) Cell doubling times (Empirical) of (**a**) Control, (**b**) MNNG1, (**c**) MNNG3, and (**d**) MNNG7. (**e, f, g and h)** Simulations were performed using the source (**e**) data-Control, (**f**) MNNG1, (**g**) MNNG3, and (**h**) MNNG7, and the cell-doubling times of the virtual cells generated by the simulations are displayed. (**i**, **j**, **k**, and **l)** Cell doubling times (Empirical) of (**i**) p53si, (**j**) p53si-MNNG1, (**k**) p53si-MNNG3, and (**l**) p53si-MNNG7. (**m**, **n**, **o**, and **p)** Results of corresponding simulations are shown; the source (**m**)

data-p53, (**n**) p53-MNNG1, (**o**) p53-MNNG3, and (**p**) p53-MNNG7. Arrow indicates the average cell-doubling time.

Supplementary Figure 11. Simulations of MD, CD, and CF. The numbers of MD (**a**), CD (**b**), and CF (**c**) events in a virtual cell population generated by the simulation (Simulation) were compared with those determined by single-cell tracking analysis (Empirical). The simulation was performed with 1,000 progenitors for a simulation time of 15,000 min and was repeated 10 times. The range of results obtained by the simulation is also indicated.

SUPPLEMENTARY MOVIES

Supplementary Movie 1. Visualization of cell density. Density of cultured cells visualized using a heat map color scale.

Supplementary Movie 2. Visualization of progress of transfection. DIC and particles with brightness of 150–254 grayscale and size of 5–30 pixels are shown.

Supplementary Movie 3. Cell-fate simulation of progeny of MD in p53-expressing cells. MD progeny and MD progeny that underwent BD are indicated in burgundy and green, respectively. Other cells are indicated in gray. The animation movie was created using data from the virtual cell-lineage database created using Source data-Control. After assigning the initial positions of the cells, the cell movement was created programmatically. When CD occurred, virtual cells were split into small particles.

Supplementary Movie 4. Cell-fate simulation of progeny of MD in p53-silenced cells. MD progeny and MD progeny that underwent BD are indicated in burgundy and green, respectively. Other cells are indicated in gray. The animation movie was created using data from the virtual cell-lineage database created using Source data-p53si. After assigning the initial positions of the cells, the cell movement was created programmatically. When CD occurred, virtual cells were split into small particles.

Supplementary Movie 5. Cell-fate simulation of p53-silenced cells in a p53-expressing cell population. The p53-silenced cells are indicated in blue. Other cells are indicated in gray. The animation movies were created using data from the virtual cell-lineage database using Source data-

Control and p53si. After assigning the initial position of the cells, cell movement was created programmatically. When CD occurred, virtual cells were split into small particles.

Supplementary Movie 6. Cell-fate simulation of p53-silenced cells in a p53-expressing cell population subjected to virtual MNNG treatment. The p53-silenced cells are indicated in blue. Other cells indicated in gray. The animation movies were created using data from the virtual cell-lineage database using Source data and p53si, and MNNG7 and p53si-MNNG7. The brightness of the im age was changed after virtual MNNG treatment at a simulation time of 10,000 min. After assigning the initial position of the cells, cell movement was created programmatically. When CD occurred, virtual cells were split into small particles.